

太行山南段洪山沟铜金矿床白云母和绿泥石特征及其找矿意义

王凯迪^{1,2}, 张娟^{1,2}, 王红³, 刘新星^{1,2}, 张勇⁴, 王丽杰^{1,2}, 李若丹^{1,2},
关子琼^{1,2}, 薛宇⁴

(1. 河北省战略性关键矿产研究协同创新中心,河北地质大学,河北石家庄 050031; 2. 河北省战略性关键矿产资源重点实验室,河北地质大学,河北石家庄 050031; 3. 河北省地矿局第九地质大队,河北邢台 054000; 4. 内蒙古自治区地质调查研究院,内蒙古呼和浩特 010041)

摘要: 洪山沟斑岩型铜金矿床是洪山多金属成矿区的典型矿床,位于华北克拉通中部南缘山西断隆武安凹陷区,矿体主要赋存于洪山正长斑岩体内。矿化中心及外围白云母和绿泥石十分发育。为探讨洪山沟铜金矿床白云母和绿泥石的成岩成矿意义,运用电子探针(EPMA)、激光剥蚀电感耦合等离子体质谱(LA-ICP-MS)分析了矿床中不同产状和成矿阶段的白云母和绿泥石。结果显示,区内绿泥石根据其分布特征可分为3类:与金属矿物共(伴)生的绿泥石(Chl-1)、由角闪石蚀变而成的绿泥石(Chl-2)及由黑云母蚀变而成的绿泥石(Chl-3)。3种绿泥石均为Fe绿泥石,指示形成于还原环境,其结构中存在Fe对Mg的置换以及Si对Al^{IV}的置换,表明绿泥石的形成受富Fe、Mg的成矿流体影响,由地质温度计计算出的绿泥石形成温度在112~272℃之间,属于中-低温热液蚀变范围。LA-ICP-MS结果显示完全蚀变的绿泥石更富Cu、S、Rb、Zn、Ti、I、U、V、Co、Ni、Sn;白云母主要有原生白云母(Ms-1)与次生白云母(Ms-2)两类,分别属于普通白云母和多硅白云母。与矿化密切相关的白云母具高Si/Fe低Al的特征,LA-ICP-MS结果显示还原环境下形成的白云母在氧化环境下形成的白云母更富V、W,暗示流体后期有大气降水的混入。综合本文研究成果认为,洪山沟铜金矿床成矿流体早期呈酸性,后期有大气降水的混入并逐渐向中性转变,铜金矿化成矿环境为近中性还原的中-低温环境,成矿流体富Fe、Mg,贫Si。

关键词: 白云母; 绿泥石; 电子探针; 洪山沟铜金矿床; 华北克拉通

中图分类号: P575.1; P575.3; P611.1 文献标识码: A 文章编号: 1000-6524(2025)04-0924-25

Characteristics of muscovite and chlorite in Hongshangou copper-gold deposit and its prospecting significance

WANG Kai-di^{1,2}, ZHANG Juan^{1,2}, WANG Hong³, LIU Xin-xing^{1,2}, ZHANG Yong⁴, WANG Li-jie^{1,2},
LI Ruo-dan^{1,2}, GUAN Zi-qiong^{1,2} and XUE Yu⁴

(1. Hebei Province Collaborative Innovation Center for Strategic Critical Mineral Research, Hebei Geology University, Shijiazhuang 050031, China; 2. Hebei Key Laboratory of Strategic Critical Mineral Resources, Hebei Geology University, Shijiazhuang 050031, China; 3. Ninth Geology Division of Hebei Bureau of Geology and Mineral Resources Exploration, Xingtai 054000, China; 4. Inner Mongolia Geological Survey Institute, Hohhot 010041, China)

收稿日期: 2024-11-05; 接受日期: 2025-04-09; 编辑: 尹淑萍

基金项目: 河北省斑岩型矿床研究重点实验室项目(HBBY202408); 河北省自然科学基金(D2024403084); 河北省战略性关键矿产研究协同创新中心开放基金资助(HGUXT-2023-15); 河北地质大学校内预研项目(KY2024QN24); 河北地质大学校内青年项目(QN202217)

作者简介: 王凯迪(2000-),女,硕士研究生,矿物学、岩石学、矿床学专业,研究方向为金属矿床成矿作用,E-mail: 1931447938@qq.com; 通讯作者: 张娟(1987-),女,博士,副教授,矿物学、岩石学、矿床学专业,研究方向为金属矿床学,E-mail: zhangjqt@126.com。

Abstract: The Hongshangou porphyry copper-gold deposit is a typical deposit in the Hongshan polymetallic metallogenetic area. It is located in the Wu'an depression of Shanxi fault uplift in the southern margin of the central North China Craton. The ore body mainly occurs in the Hongshan syenite porphyry. Muscovite and chlorite are well developed in the mineralization center and periphery. In order to discuss the diagenesis and mineralization significance of muscovite and chlorite in Hongshangou copper-gold deposit, electron probe microanalysis (EPMA) was used to analyze muscovite and chlorite in different occurrences and metallogenetic stages of the deposit. The results show that the distribution characteristics of chlorite in the mining area can be divided into three categories: chlorite associated with metal minerals (Chl-1), chlorite altered from hornblende (Chl-2) and chlorite altered from biotite (Chl-3). The three chlorites are all Fe chlorites, indicating that they were formed in a reducing environment. The replacement of Fe to Mg and the replacement of Si to Al^{IV} in the structure indicate that the formation of chlorites is affected by Fe- and Mg-rich ore-forming fluids. The formation temperature of chlorite calculated by geological thermometer is between 112~272°C, which belongs to the range of medium-low temperature hydrothermal alteration, LA-ICP-MS results show that the completely altered chlorite is richer in Cu, Sn, Rb, Zn, Ti, V, Sr, V, Co, Ni and Sn. Muscovite mainly includes primary muscovite (Ms-1) and secondary muscovite (Ms-2), which belong to ordinary muscovite and polysilicic muscovite respectively. The muscovite closely related to mineralization has the characteristics of high Si, Fe and low Al, LA-ICP-MS results show that the muscovite formed in the reducing environment is richer in V and W than the muscovite formed in the oxidizing environment, suggesting the mixing of meteoric water in the later stage of the fluid. Based on the research results of this paper, the ore-forming fluid of Hongshangou copper-gold deposit is acidic in the early stage and gradually changes to neutral in the later stage. The ore-forming environment of copper-gold deposit is near neutral and reduced medium-low temperature environment. The ore-forming fluid is rich in Fe, Mg and poor in Si.

Key words: muscovite; chlorite; electron probe microanalysis; Hongshangou porphyry copper-gold deposit; North China Craton

Fund support Key Laboratory of Porphyry Deposit Research in Hebei Province (HBBY202408); Natural Science Foundation of Hebei Province (D2024403084); Hebei Province Strategic Key Minerals Research Collaborative Innovation Center Open Fund (HGUXT-2023-15); Hebei University of Geosciences Campus Pre-research Project (KY2024QN24); The Youth Project of Hebei University of Geosciences (QN202217)

绿泥石为含水层状铁-镁-铝硅酸盐矿物,形成于高-中-低变质作用、成岩作用和热液蚀变作用等各种地质环境中(Wiewióra and Weiss, 1990; Zane and Weiss, 1998; Li *et al.*, 2022),在自然界中广泛分布,与铜、金、铀等多金属矿床成矿作用密切相关(张展适等, 2007; 王小雨等, 2014; Basori *et al.*, 2022; Feng *et al.*, 2022; 曾淑明等, 2023)。不同成因的绿泥石的成分有较大差异,通过分析其化学成分能够反演形成时所处环境的物理化学条件。Cathelineau(1988)在分析绿泥石的成分和温度之间的关系时发现绿泥石中的Al^{IV}含量与其形成时温度存在正相关性,由此提出绿泥石固溶体温度计。近年来,国内外学者对绿泥石的形成环境、机制与温度进行了大量研究,探讨绿泥石与多金属矿床矿化之间的关系并取得大量成果(赵友东等, 2016; Xiao *et*

al., 2018; Wu *et al.*, 2019; Zhang *et al.*, 2020)。

白云母是具有二八面体的层状硅酸盐矿物,在斑岩型矿床、矽卡岩型矿床等矿床中广泛发育,是热液作用过程的产物(Keppler, 1993; Černý *et al.*, 2003; 马万伟等, 2020)。白云母由于其结构的特殊性会发生类质同象替换,包括Tschermark置换($\text{Al}^{\text{IV}} \leftrightarrow \text{Si} = \text{Al}^{\text{VI}} \leftrightarrow \text{Fe} + \text{Mg}$)及层间 $\text{Na}^+ + \text{Ca}^{2+} \leftrightarrow \text{K}^+$ 置换(Thompson *et al.*, 2009),其种类、结构特征以及矿物地球化学特征可以指示流体演化程度及过程(Neiva, 2013; Laakso *et al.*, 2016; Schirra *et al.*, 2022; 付建刚等, 2023; 楚翔凯等, 2023),因此,通过研究白云母化学成分及结构有助于了解各类型矿床的成矿流体演化与成矿过程(Tischendorf *et al.*, 1997; Li *et al.*, 2015; Legros *et al.*, 2018; Yin *et al.*, 2019; 王葆华等, 2021)。

太行山南段是我国东部重要的金属成矿区,构造上位于大兴安岭-太行山构造岩浆带南段(权瑞等,2016)。中生代大规模构造-岩浆活动到燕山期造山过程中的大规模岩浆活动使区内形成一系列碱性-钙碱性侵入岩,为形成金属矿床提供了条件(翟明国等,2005;吴福元等,2008;张海东等,2014;息朝庄等,2021)。受印支期古西伯利亚板块向南俯冲、古扬子板块向北仰冲与燕山期太平洋板块向西俯冲的影响,我国东部处于强拉应力区,导致区内断裂与褶皱均发育,西部北北东向紫山-鼓山大断裂以及北东向褶皱为区内主要容矿构造(刘昕曜,2016)。该区地层剖面较为完整,依次为太古宇下赞皇群,中元古界长城系,古生界寒武系、奥陶系、石炭系、二叠系,中生界三叠系、白垩系,新生界古近系及第四系(刘昕曜,2016)。前人研究表明,洪山岩体分3次岩浆活动:第1次为火山喷发活动,形成一套粗面质火山岩系;第2次为岩浆侵入,主要形成辉石(角闪)正长岩系列;第3次为钙碱性系列岩石大规模侵入,形成以浅色正长岩为主的洪山岩体的主体。洪山沟铜矿化的发生应与正长斑岩侵位后的岩浆热液活动有关(李玉成等,2016;李随民等,2022)。

斑岩型矿床是产于岩浆弧与陆缘弧环境、成因上与中酸性浅成-超浅成侵入密切相关的几类岩浆-热液矿床,流体演化一直是斑岩型矿床研究的热点问题(陈彦青等,2007;侯增谦等,2007;Richards et al., 2012; Richards, 2015; Hou et al., 2015; Mernagh et al., 2020)。随着研究手段不断发展,对流体演化的研究逐渐精细化,通过流体包裹体、硫化物成分分析等手段对流体演化过程已有较为清晰的认知(Chang et al., 2018; Wang et al., 2018; Yang et al., 2022; Adegoke et al., 2022),普遍认为斑岩型矿床成矿流体具高温、高氧逸度、高盐度的特征,通常含有水蒸气、二氧化碳等挥发性物质(Pak et al., 2004; 李进文等,2006)。然而,部分研究表明,斑岩型成矿流体的特征存在显著差异,例如一些矿床的成矿流体在初期可能表现为低氧逸度和还原性(Sillitoe, 1972, 2010)。流体性质对矿床规模具有重要控制作用,初期低氧逸度、还原性流体通常形成规模较小的矿床。因此,流体特征及其演化过程对矿床的形成起着决定性作用。蚀变矿物作为成矿流体与围岩相互作用的直接产物,其类型和组合特征对揭示成矿环境和流体演化具有重要意义。绿泥石和白云母是斑岩型矿床中常见的蚀变矿物,其化

学成分和结构特征能够有效反映成矿流体的物理化学条件。例如,绿泥石的成分变化可指示成矿温度及流体性质,而白云母中Si、Al的置换关系则能够反映流体的pH值、氧逸度及水岩反应过程。通过研究这些蚀变矿物的类型及其地质意义,能够深入揭示成矿流体的演化路径及其对铜金成矿的控制作用。

洪山沟铜矿位于邯郸市永年区西侧洪山岩体北部,受洪山古火山机构与紫山-鼓山断裂控制,矿体主要分布于洪山沟正长斑岩内。目前,洪山沟铜金矿床的地质特征(常浩等,2020)、成岩成矿时代(权瑞等,2016;李随民等,2022)、成岩成矿作用(权瑞等,2016;白富生,2022)、岩浆演化(张波等,2020)等方面研究成果较多,但洪山沟铜金矿床蚀变矿物类型及其组合分带特征尚未厘清,成矿环境以及流体演化也缺乏详细研究。因此,本文基于野外地质调查,利用电子显微镜观察、电子探针化学分析(EPMA)、激光剥蚀电感耦合等离子体质谱(LA-ICP-MS)对洪山沟铜金矿床中绿泥石和白云母的类型、组分、形成温度、环境及其形成机制进行了系统研究,以期查明与绿泥石和白云母有关的各成矿阶段成矿流体的性质,约束洪山沟铜金矿床成矿流体的演化特征及铜金沉淀的物理化学环境。

1 区域地质背景

洪山多金属成矿区位于华北板块中部太行山南段,大地构造位置属于山西断隆太行山拱断束中的武安凹断束东部,东邻太行山断裂带(图1)(史志伟等,2020;崔晓亮等,2022)。区域地层为一套以海相沉积为主的盖层岩系。区域内中生代燕山期岩浆活动强烈,分布广泛。岩浆岩主要有武安岩体、矿山岩体及洪山杂岩体(Xu, 2001; 王春光等, 2011; 息朝庄等, 2021)。其中武安岩体以闪长岩为主,矿山岩体以闪长岩、二长岩为主,洪山杂岩体中心侵入为正长岩(尹明等, 2014; 息朝庄等, 2021),向南、北两侧分别为晶屑凝灰岩、凝灰熔岩、黑云辉石粗面岩、黑云辉石粗面斑岩及黑云正长辉石岩、黑云辉石正长岩等。该区构造活动强烈,断裂及褶皱具明显中生代滨太平洋域构造特征,褶皱构造为新城-武安向斜和鼓山背斜,断裂为邯郸大断裂与紫衫-鼓山大断裂,均为北北东向断裂(许文良等, 1990a, 1990b; 耿国建等, 2023; 杨长青等, 2023),紫山-鼓山断裂及其他一级构造为本区重要的导矿构造,许多金矿

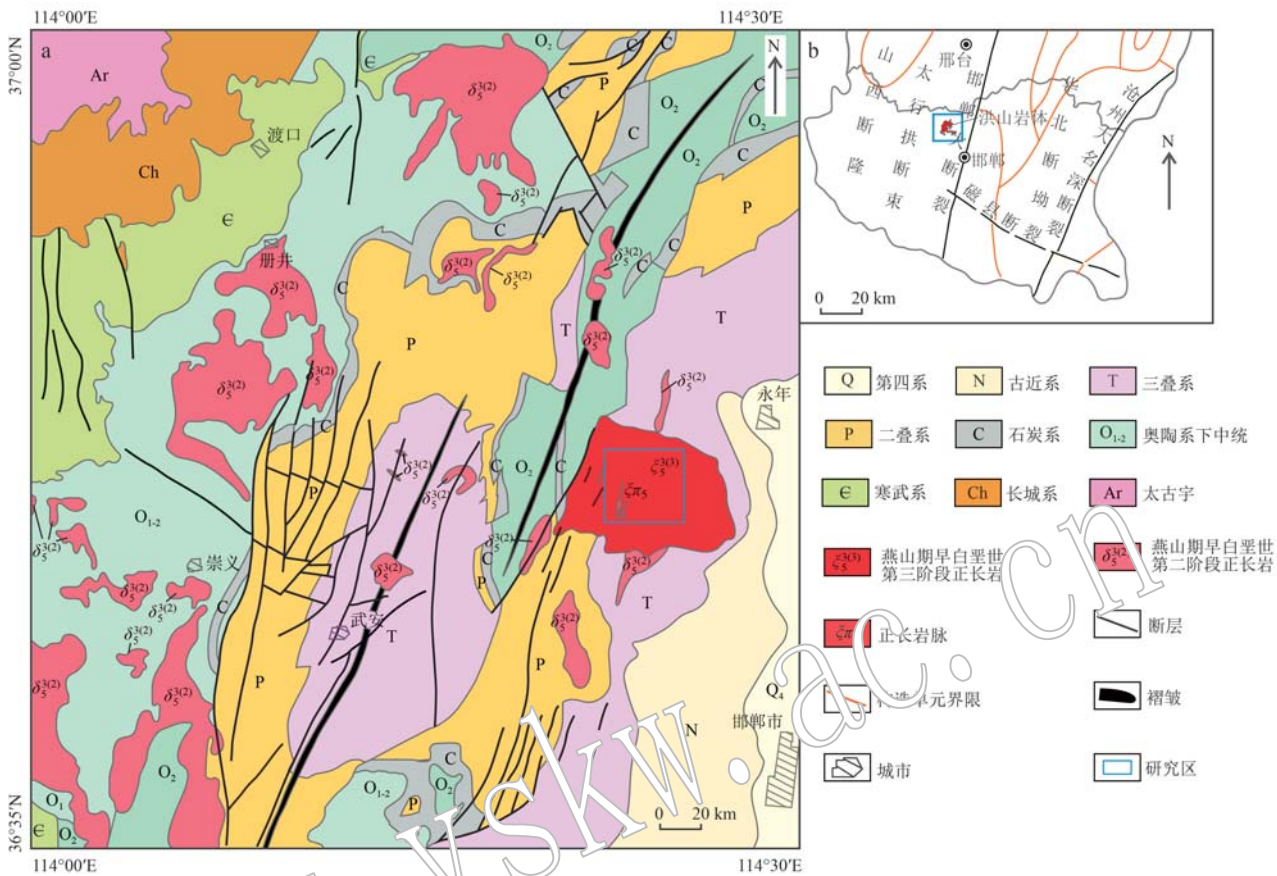


图 1 洪山岩体与其周围区域地质图(a)及大地构造位置图(b)(据刘昕耀, 2016 修改)
Fig. 1 Geological map of Hongshan rock mass and its surrounding area (a) and geotectonic location map (b)
(modified from Liu Xinyao, 2016)

化点沿该断裂带分布。

区域矿产较丰富,以煤、铁矿种为主,金、铜多金属矿(化)点分布于洪山岩体及其周边,主要有营里、娄里、泉上金矿点以及洪山沟、里三窑、娄里金矿等。

2 矿床地质特征

洪山沟斑岩型铜金矿床位于邯郸市洪山岩体北部,分布于邯郸大断裂与紫山-鼓山大断裂之间的西北东向构造岩浆岩带内(图2)(常浩等, 2020)。

洪山岩体主要由碱性正长岩类组成,岩体与围岩之间呈侵入关系。锆石U-Pb年龄显示洪山岩体形成于早白垩世(周凌等, 2005; 权瑞等, 2016),可分为喷出相-超浅成侵入相、侵入相两种岩相。喷出相主要分布在岩体的南北两侧边部,呈近东西向带状分布,岩石类型主要为凝灰岩、粗安玢岩、粗面岩、黑云辉石粗面岩和辉石-粗面岩等中性及中偏碱性

岩浆岩;侵入相主要为霓辉正长岩和正长岩。

洪山沟铜金矿床的矿体主要赋存于含铜正长斑岩内,斑岩体矿化明显,主要为浸染状及细脉浸染状。矿石类型为斑岩型铜矿石,矿石矿物以黄铜矿为主,蓝辉铜矿次之,脉石矿物有条纹长石、霓辉石、石英、黑云母、绢云母、角闪石、霓石或方解石等。矿石结构为他形粒状结构、充填交代结构以及反应边结构,构造主要呈浸染状及细脉浸染状(刘昕耀, 2016)。矿床按期次可分为:① 霓辉石-硫化物阶段,主要矿物为霓辉石、黄铁矿、黄铜矿;② 浸染状硫化物阶段,为主成矿阶段,黄铁矿、黄铜矿等硫化物呈浸染状分布在含矿正长斑岩中,与霓辉石、磁铁矿共生;③ 石英-黄铁矿阶段,主要矿物为石英和黄铁矿,二者常呈细脉产出。围岩蚀变主要为绢云母化、绿泥石化、钾化、硅化及黑云母化等。矿体中心以硅化及钾化为主,外围以绢云母化及绿泥石化为主。铜矿化与硫化物及硅化密切相关(姚士新等, 1993; 常浩等, 2020)。

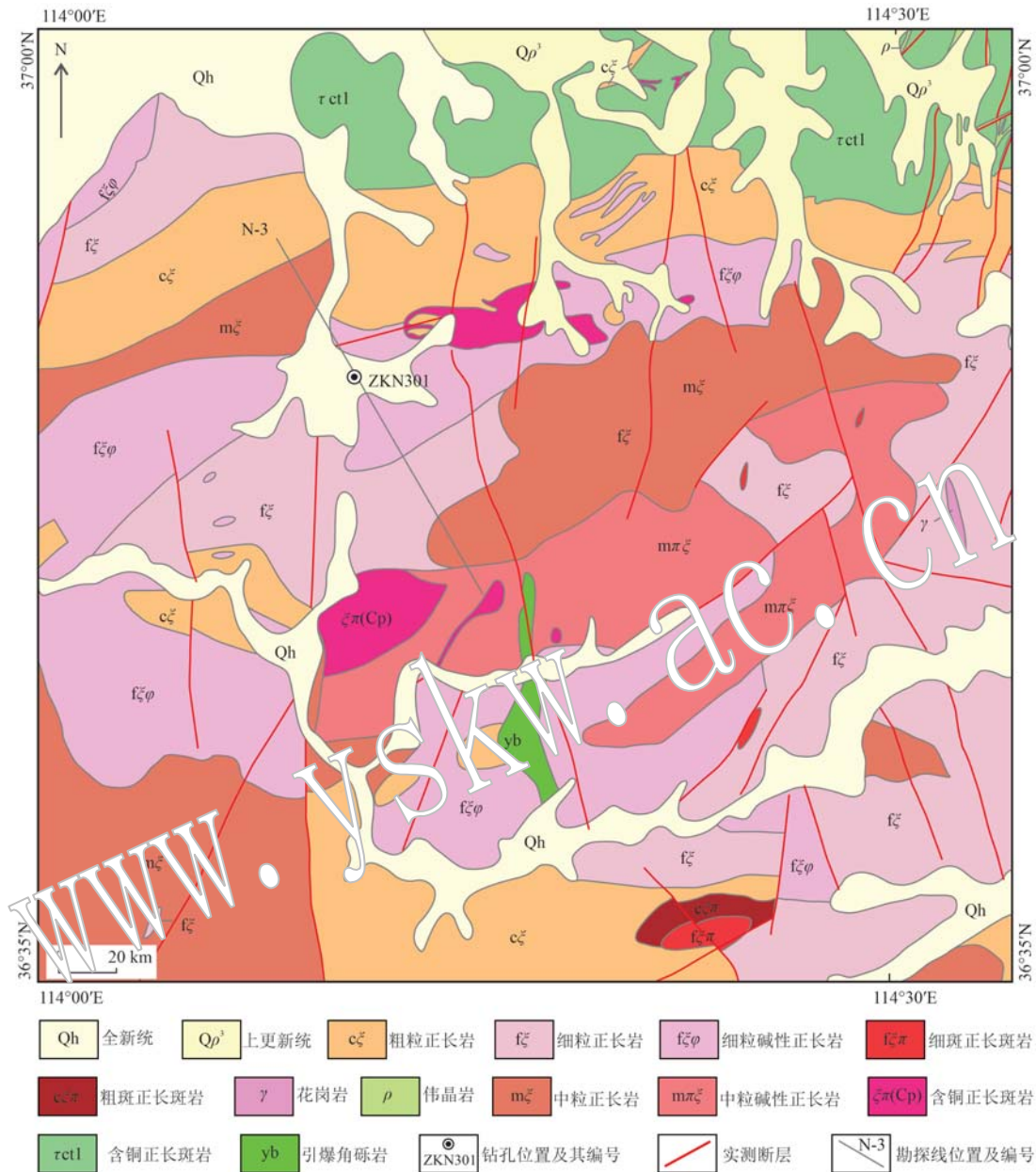


图2 洪山沟矿区地质图(据常浩等, 2017修改)

Fig. 2 Geological map of Hongshangou mining area (modified from Chang Hao et al., 2017)

3 蚀变矿物岩相学特征

3.1 绿泥石类型及分布特征

绿泥石是洪山沟铜金矿床中重要的热液蚀变矿物, 在洪山沟铜金矿床的矿体与岩体中广泛分布, 尤其在矿体发育部位发育。通过室内镜下鉴定, 根据绿泥石蚀变类型及分布特征, 将洪山沟铜金矿床中绿泥石分为: ①与金属矿物共生的完全蚀变型绿泥

石(Chl-1), 是矿区绿泥石的主要发育类型, 绿泥石在单偏光下呈灰绿色-绿色, 与金属矿物和长石共生, 为流体交代暗色矿物形成(图3a、3b、3c); ②角闪石蚀变型的绿泥石(Chl-2), 发育程度次于Chl-1, 绿泥石呈细小鳞片状, 单偏光镜下呈绿色, 为流体不完全交代角闪石形成, 与角闪石共生(图3d、3e); ③黑云母蚀变型绿泥石(Chl-3), 在矿区不发育。绿泥石为细小鳞片状, 单偏光下为墨绿色, 为流体不完全交代黑云母形成, 与黑云母共生(图3f)。

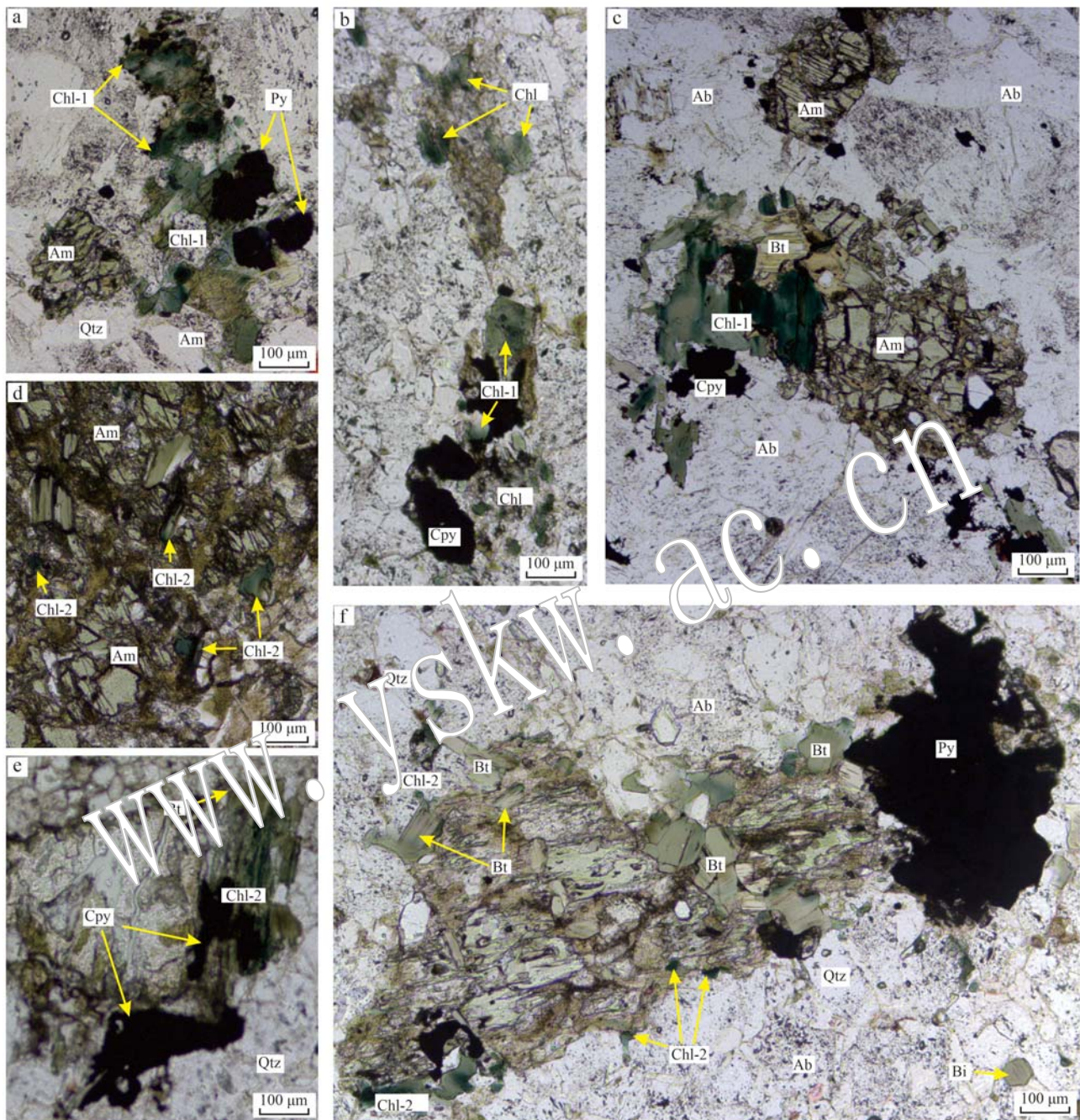


图3 绿泥石电子显微镜单偏光照片

Fig. 3 Typical microphotographs (plane-polarized light) of chlorite

a—Chl-1, 绿泥石完全交代暗色矿物, 与角闪石、长石、石英、黄铜矿共生; b—Chl-1, 绿泥石完全交代暗色矿物, 可见不完全交代角闪石骸晶, 与角闪石、长石、石英、黄铜矿共生; c—Chl-1, 绿泥石完全交代暗色矿物, 可见不完全交代黑云母骸晶, 与角闪石、黑云母、长石、石英、黄铜矿共生; d—Chl-2, 颗粒较小, 与角闪石共生; e—Chl-2, 角闪石部分蚀变为绿泥石, 与黑云母、黄铜矿共生; f—Chl-3, 黑云母部分蚀变为绿泥石, 与黑云母、黄铁矿共生; Ab—钠长石; Am—角闪石; Bt—黑云母; Chl—绿泥石; Cpy—黄铜矿; Py—黄铁矿; Qtz—石英

a—Chl-1, chlorite completely metasomatism dark minerals, and coexists with amphibole, feldspar, quartz, and chalcopyrite; b—Chl-1, chlorite completely metasomatism dark minerals, visible incomplete metasomatism amphibole skeleton crystal, and amphibole, feldspar, quartz, chalcopyrite symbiosis; c—Chl-1, chlorite completely metasomatism dark minerals, visible incomplete metasomatism biotite crystal, and hornblende, biotite, feldspar, quartz, chalcopyrite symbiosis; d—Chl-2, small particles, symbiotic with hornblende; e—Chl-2, hornblende is partially altered into chlorite, which is symbiotic with biotite and chalcopyrite; f—Chl-3, biotite partially altered into chlorite, coexisting with biotite and pyrite; Ab—albite; Am—hornblende; Bt—biotite; Chl—chlorite; Cpy—chalcopyrite; Py—pyrite; Qtz—quartz

3.2 白云母的类型及分布特征

热液白云母是洪山沟铜金矿床中另一广泛发育的蚀变矿物,白云母的成因及成分差异可指示洪山沟铜金矿床成矿流体的演化过程。白云母岩相学特征及电子探针结果可以判定白云母成因。原生白云母一般呈自形-半自形,矿物颗粒粗大,端面清晰,不与其他矿物呈反应关系,不含包裹体等,而次生白云母则相反,通过镜下白云母形态将洪山沟铜金矿床中的白云母分为原生白云母(Ms-1)与次生白云母(Ms-2)。

根据其矿物组合将原生与次生白云母进一步详细划分。原生白云母:①与长石共生的片状白云母Ms-1.1。干涉色主要为蓝色,呈集合体或片状在长石边缘产出(图4a、4b);②与方解石共生的片状白云母Ms-1.2,干涉色为紫色、橙色,呈片状与碳酸盐矿物伴生(图4c、4d)。次生白云母:①与长石共生的细小鳞片状白云母Ms-2.1。干涉色为橙黄色、蓝色,颗粒较细,叠加于长石之上(图4e、4f);②与长石、黄铜矿共生的片状白云母Ms-2.2。较为发育,干涉色多为蓝色、橙红色;颗粒较细,叠加于长石之上,与黄铜矿共生(图4g);③与方解石、黄铜矿共生的鳞片状-片状白云母Ms-2.3。干涉色为绿色、蓝色以及紫色,与方解石共生,呈片状或鳞片状,与黄铜矿、黄铜矿共生(图4h、4i)。

4 测试方法

本次研究针对绿泥石、白云母采用电子探针(EPMA)、激光剥蚀电感耦合等离子体质谱(LA-ICP-MS)分析其主微量元素变化。

绿泥石、白云母的EPMA分析在中国地质科学院矿产资源研究所电子探针实验室完成,电子探针测试仪器为日本岛津公司的EPMA-8320,加速电压15 kV;电流20 nA;束斑直径5 μm;校正ZAF;温度25°C;湿度55%~60%。

绿泥石、白云母的微量元素分析在河北省战略性关键矿产资源重点实验室完成,实验仪器采用搭载Laurin Technic S155样品池和GeoStar μGISTM软件的澳大利亚RESolution-LR型ArF准分子激光剥蚀系统,质谱仪为美国赛默飞iCAP RQ型等离子体质谱仪,按照其标准操作规程,采用的激光束斑大小为50 μm,能量密度为3 J/cm,频率为8 Hz,氦气为载气。元素含量采用NIST610作外标,²⁹Si为内标

元素进行校正,实验测得数据采用ICPMsDataCal软件进行同位素比值及元素含量的计算。

5 绿泥石化学成分特征

由于本次研究的绿泥石颗粒比较细小且与其他矿物形成伴生关系,化学成分极易受混染,影响电子探针结果(Inoue, 1995),经前人研究证明绿泥石的($\text{Na}_2\text{O}+\text{K}_2\text{O}+\text{CaO}$)含量<0.5%表明分析过程中未发生其他矿物的混染(Hillier, 1993; Zang and Fyfe, 1995),经人工筛查后确认洪山沟铜多金属矿床3种绿泥石样品的($\text{Na}_2\text{O}+\text{K}_2\text{O}+\text{CaO}$)含量均小于0.5%,测试结果有效。各类型绿泥石化学成分含量详见表1,其中电子探针数据显示样品中 SiO_2 的含量在26.41%~34.41%之间, Al_2O_3 的含量在8.24%~13.16%之间,差别较小;FeO含量在25.53%~35.67%之间, MgO 含量在10.58%~18.08%之间,差别较大;此外,Chl-1、Chl-2、Chl-3中FeO平均含量分别为30.00%、25.34%、25.73%, MgO 平均含量分别为13.51%、17.42%、13.59%,说明绿泥石随成矿流体演化发生离子置换。

绿泥石LA-ICP-MS分析结果详见表2,根据LA-ICP-MS结果,绿泥石Li、Sn、Ga、Sc、Ti、V、Cr、Co、Ni、Cu、Zn、As、Rb、Sr等元素的含量为 0.01×10^{-6} ~ 1800×10^{-6} ,Nb、Y、La、Nd等低于检出限。相较于未完全蚀变的绿泥石,完全蚀变的绿泥石具有更高的Cu、Sn、Rb、Zn、Ti、Li、Sr、V、Co、Ni、Sn含量。

5.1 绿泥石温度计算结果

前人研究发现绿泥石成分中 Al^{IV} 含量与温度之间存在正相关关系,因此提出绿泥石固溶体温度计以研究成矿过程中热液的温度变化(Cathelineau and Nieva, 1985),本次研究使用Winccac绿泥石计算软件计算经验性绿泥石温度计,以此评估洪山沟铜金矿床中绿泥石的结晶温度。在经验性温度计中,以Kranidiotis等(1987)(TKML87-Al^{IV})及Cathelineau(1988)(TC88-Al^{IV})方法计算出的绿泥石温度范围较为集中,Kavalieris等(1990)(TK90-Si)、Jowett(1991)(TJ91-Al^{IV})、Hiller和Velde(1991)(THV91-Al^{IV})方法计算出的绿泥石温度差别较大,详细计算结果见表3。

5.2 绿泥石 $\text{Al}/(\text{Al}+\text{Mg}+\text{Fe}^{2+})$ 与 $\text{Fe}/(\text{Fe}+\text{Mg})$ 值

$\text{Al}/(\text{Al}+\text{Mg}+\text{Fe}^{2+})$ 值可以判别绿泥石与母岩

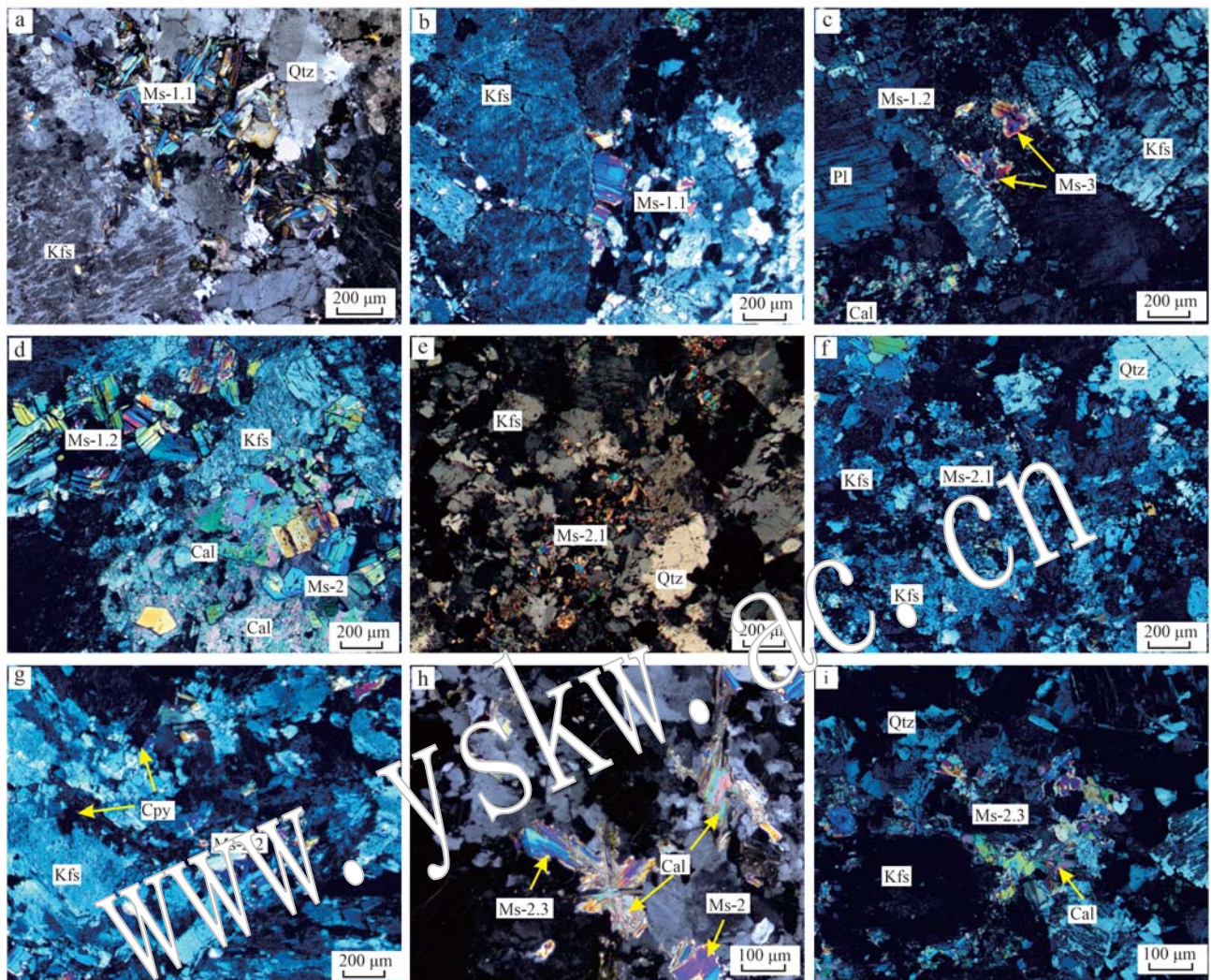


图4 白云母电子显微镜正交偏光照片

Fig. 4 Typical microphotographs (cross-polarized light) of muscovite

a—Ms-1.1, 白云母集合体与钾长石共生; b—Ms-1.1, 片状白云母与钾长石共生; c—Ms-1.2, 片状白云母与碳酸盐矿物、斜长石共生; d—Ms-1.2, 片状白云母集合体与碳酸盐、钾长石共生; e—Ms-2.1, 鳞片状白云母叠加钾长石之上, 与石英共生; f—Ms-2.1, 鳞片状白云母叠加钾长石之上, 与石英共生; g—Ms2.2, 鳞片状白云母叠加于长石之上, 与碳酸盐矿物、黄铜矿共生; h—Ms-2.3, 片状白云母与碳酸盐矿物、黄铜矿共生; i—Ms-2.3, 片状白云母集合体与碳酸盐矿物、黄铜矿共生; Cal—方解石; Cpy—黄铜矿; Kfs—钾长石; Ms—白云母; Pl—斜长石; Qtz—石英

a—Ms-1.1, muscovite aggregates coexist with potassium feldspar; b—Ms-1.1, flaky muscovite coexists with potassium feldspar; c—Ms-1.2, flaky muscovite coexists with carbonate minerals and plagioclase; d—Ms-1.2, flaky muscovite aggregates coexist with carbonate and potassium feldspar; e—Ms-2.1, scaly muscovite superimposed on potassium feldspar, coexists with quartz; f—Ms-2.1, scaly muscovite superimposed on potassium feldspar, coexists with quartz; g—Ms2.2, scaly muscovite superimposed on feldspar, coexists with carbonate minerals and chalcopyrite; h—Ms-2.3, flaky muscovite coexists with carbonate minerals and chalcopyrite; i—Ms-2.3, flaky muscovite aggregates coexist with carbonate minerals and chalcopyrite; Cal—calcite; Cpy—chalcopyrite; Kfs—potassium feldspar; Ms—muscovite; Pl—plagioclase; Qtz—quartz

之间的关系,一般认为 $Al/(Al+Mg+Fe) > 0.35$ 为泥质岩蚀变而成, $Al/(Al+Mg+Fe) < 0.35$ 则为铁镁质矿物蚀变(Laird, 1988),表3显示各类型绿泥石的 $Al/(Al+Mg+Fe)$ 值均小于0.35,表明淇山沟铜金矿床中的绿泥石均为铁镁质矿物蚀变。 $Fe/(Fe+Mg)$

值可判断绿泥石形成环境,一般认为 $Fe/(Fe+Mg)$ 值越大,环境的还原性越高 [$Fe/(Fe+Mg) > 0.5$],易形成Fe绿泥石(Inoue, 1952; Bryndzia and Scott, 1987; 郭国林等, 2012), Chl-1的 $Fe/Fe+Mg$ 值在0.57~0.65之间,Chl-2的 $Fe/(Fe+Mg)$ 值在0.44~0.49之

表1 洪山沟铜金矿床绿泥石电子探针分析结果
Table 1 Electron microprobe analyses of chlorite from the Hongshangou copper-gold deposit

 $w_B/\%$

类型 样品号	Chl-1						Chl-2						Chl-3	
	259-1	259-2	416.1-1	416.1-2	416.1-3	416.1-4	264.3-1	346.13-1	416.1-1	419.5-1	419.5-2	419.5-3	387.2-1	387.2-2
SiO ₂	26.41	27.06	28.81	28.66	27.88	28.12	30.20	30.31	29.22	29.17	29.58	28.58	34.24	34.41
TiO ₂	0.12	0.10	0.22	0.21	0.20	0.20	0.45	0.35	0.06	0.31	0.30	0.30	0.39	0.39
Al ₂ O ₃	12.03	9.75	11.38	10.91	11.32	10.80	8.73	8.99	11.47	12.66	12.66	13.16	8.24	8.40
Cr ₂ O ₃	0.09	0.18	0.17	0.28	0.19	0.11	0.28	0.18	0.48	0.36	0.30	0.26	1.10	0.51
FeO	35.10	35.67	31.42	31.08	31.98	32.30	25.53	25.73	26.38	26.26	26.01	26.06	25.69	25.78
MnO	1.45	1.15	1.13	1.04	1.24	1.17	0.98	0.66	1.41	1.03	1.01	1.10	1.41	1.39
MgO	10.58	12.20	12.67	12.95	12.43	12.57	18.08	18.63	16.06	15.55	15.75	15.52	13.52	13.66
CaO	0.06	0.05	0.30	0.36	0.36	0.30	0.17	0.17	0.32	0.51	0.54	0.33	0.27	0.28
Na ₂ O	0.02	0.04	0.03	0.04	0.06	0.03	0.00	0.03	0.06	0.06	0.09	0.08	0.05	0.03
K ₂ O	1.16	0.28	0.01	0.02	0.70	0.34	2.32	2.13	0.59	2.52	2.24	2.74	1.04	1.10
总和	87.19	86.72	86.26	85.74	86.61	86.08	87.10	87.59	86.37	88.67	88.66	88.36	86.29	86.30
Si	3.03	3.08	3.23	3.24	3.16	3.20	3.15	3.30	3.21	3.15	3.17	3.09	3.72	3.73
Ti	0.01	0.01	0.02	0.02	0.02	0.02	0.03	0.03	0.00	0.03	0.02	0.01	0.03	0.03
Al	1.63	1.31	1.51	1.45	1.51	1.45	1.60	1.15	1.49	1.61	1.60	1.6	1.06	1.07
Cr	0.01	0.02	0.01	0.03	0.02	0.01	0.03	0.02	0.04	0.03	0.03	0.02	0.09	0.04
Fe ²⁺	3.28	2.97	2.95	2.94	3.03	3.07	2.42	2.34	2.43	2.37	2.33	2.36	2.34	2.34
Mn	0.14	0.11	0.11	0.10	0.12	0.11	0.09	0.06	0.13	0.09	0.09	0.10	0.13	0.13
Mg	1.81	2.07	2.12	2.18	2.10	2.13	2.55	3.02	2.50	2.52	2.50	2.19	2.21	
Ca	0.01	0.01	0.04	0.04	0.04	0.04	0.05	0.02	0.04	0.06	0.06	0.04	0.03	0.03
Na	0.00	0.01	0.01	0.01	0.01	0.01	0.01	0.01	0.01	0.01	0.02	0.02	0.01	0.01
K	0.17	0.04	0.00	0.00	0.10	0.05	0.09	0.09	0.08	0.35	0.31	0.38	0.14	0.15
F	0.11	0.14	0.07	0.10	0.13	0.0	0.11	0.24	0.18	0.11	0.07	0.08	0.20	0.22
Cl	0.00	0.00	0.00	0.01	0.00	0.00	0.01	0.00	0.01	0.01	0.02	0.00	0.00	0.00
X _{Fe}	0.64	0.59	0.58	0.57	0.59	0.59	0.49	0.44	0.48	0.49	0.48	0.49	0.41	0.40
X _{Mg}	0.36	0.41	0.42	0.43	0.41	0.41	0.51	0.56	0.52	0.51	0.52	0.51	0.38	0.38
Fe/(Fe+Mg)	0.60	0.52	0.55	0.57	0.59	0.59	0.49	0.44	0.48	0.49	0.48	0.49	0.52	0.51
Al/(Al+Mg+Fe ²⁺)	0.24	0.21	0.23	0.22	0.23	0.22	0.24	0.18	0.23	0.25	0.25	0.26	0.19	0.19
NaO+K ₂ O+CaO	0.19	0.06	0.08	0.10	0.20	0.13	0.30	0.34	0.17	0.48	0.45	0.47	0.22	0.22
Al+Mg+Fe	6.81	6.78	6.57	6.57	6.64	6.65	6.56	6.52	6.54	6.48	6.45	6.54	5.58	5.63

表2 洪山沟铜金矿床绿泥石LA-ICP-MS分析结果
Table 2 LA-ICP-MS analysis results of chlorite in Hongshangou copper-gold deposit

 $w_B/10^{-6}$

类型	编号	Li	Sn	Ga	Sc	Ti	V	Cr	Co	Ni	Cu	Zn	As	Rb	Sr
Chl-1	416.1-1	123.00	1.38	20.46	16.32	493.08	121.53	29.02	22.83	40.48	2.26	624.13	0.48	309.03	327.45
	419.5-1	426.74	6.79	24.91	19.00	1815.11	321.74	21.7	61.91	67.26	0.66	916.93	0.05	1393.04	6.91
	264.3-1	161.16	0.08	18.08	1.76	29.62	12.35	50.01	0.19	0.06	0.90	9.43	0.50	133.89	14.48
	264.3-2	101.20	0.11	10.68	1.40	21.66	12.18	6.08	0.27	0.36	1.53	7.75	0.10	116.36	6.45
Chl-2	264.3-3	106.90	0.46	13.82	2.72	327.4	74.74	12.99	3.00	1.57	1.85	76.65	0.14	175.15	17.97
	346.13-1	17.25	0.43	9.53	3.72	6.98	23.65	160.53	4.07	6.46	1.33	64.87	0.04	10.13	139.29
	387.2-1	243.00	9.55	29.00	47.07	1630.04	357.13	166.79	47.12	62.73	2.71	1411.14	0.79	663.65	34.39

间, Chl-3 的 Fe/(Fe+Mg) 值为 0.52、0.51, 表明洪山沟铜金矿床主要成矿环境为还原性, 成矿流体经历了由氧化性→中性→还原性的演化过程。

5.3 绿泥石离子间置换关系

绿泥石中的离子常出现置换现象, 一般为 Al 与

四面体上的 Si、八面体上的 Fe 和 Mg 相互置换, 形成四次配位 Al^{IV}、六次配位 Al^{VI}, Fe、Mg 之间也可按任意比例互相置换 (Inoue et al., 2009)。根据绿泥石电子探针结果投图, 结果表明在 Al^{IV}-Si 图解中两者出现明显的线性负相关关系 (图5a), 说明在绿泥石

表3 洪山沟铜金矿床绿泥石不同地温计计算结果 ℃
Table 3 Calculation results of different geothermometers in the Hongshangou copper-gold deposit

类型	样品号	TKML87-Al ^{IV}	TC88-Al ^{IV}	TK90-Si	TJ91-Al ^{IV}	THV91-Al ^{IV}
Chl-1	259-1	272.00	250.00	150.00	261.00	158.00
	259-2	258.00	233.00	137.00	243.00	132.00
	416.1-1	243.00	185.00	113.00	194.00	58.00
	416.1-2	242.00	183.00	112.00	192.00	54.00
	416.1-3	240.00	209.00	122.00	218.00	94.00
	416.1-4	242.00	196.00	117.00	206.00	75.00
Chl-2	264.3-1	197.00	160.00	107.00	164.00	-
	346.13-1	199.00	164.00	108.00	169.00	-
	416.1-1	221.00	192.00	115.00	198.00	68.00
	419.5-1	235.00	213.00	125.00	219.00	101.00
	419.5-2	229.00	204.00	120.00	210.00	88.00
Chl-3	419.5-3	246.00	230.00	135.00	236.00	127.00
	387.2-1	115.00	-	163.00	164.00	176.00
	387.2-2	112.00	-	167.00	166.00	176.00

注: -表示未计算出结果。

中存在大量 Al^{IV} 对 Si 的置换(王炜等, 2021); 在 Fe-Mg 图解中两者出现明显负相关关系(图 5c), 说明在绿泥石中除存在 Al^{IV} 对 Si 的置换外还存在 Fe 与 Mg 的置换; Al^{VII}-Al^{IV} 图解中两者出现明显线性负相关关系(图 5e), 说明 Al^{IV} 对 Si 置换的同时出现 Fe-Mg 对 Al^{VII} 置换(Xie et al., 1997; 王小雨等, 2014)。Kranidiotis 等(1987)研究发现, Al^{IV} 随着 Fe/(Fe+Mg) 的升高而升高, Fe/(Fe+Mg)-Al^{IV} 图解中出现相同趋势(图 5b), 说明绿泥石中 Al^{IV}-Si 置换的同时出现 Fe-Mg 置换并使更多的 Fe 置换 Mg 进入绿泥石(Kranidiotis et al., 1987; Xie et al., 1997)。绿泥石中的离子出现相互置换的现象主要因所处环境的温度及酸碱度发生变化(艾永富等, 1998)。

5.4 绿泥石中主要阳离子与 Mg 的关系

前人研究证明若 Fe²⁺、Fe³⁺、Si、Mn 等阳离子均与 Mg 呈负相关关系, 表明绿泥石形成于同一期热液活动(Battaglia, 1999)。洪山沟铜金矿床中绿泥石主要阳离子与 Mg 的关系图中, 仅 Al/Fe²⁺ 与 Mg 呈弱负相关(图 6a、6b), 其他阳离子与 Mg 相关性不明显(图 6c、6d), 说明本区绿泥石经历了多期次的热液演化活动。

6 白云母化学成分特征

白云母电子探针分析结果详见表 4, 根据电子探针结果, Ms-1.1 的 SiO₂ 含量(44.00%~45.21%)

较 Ms-1.2(43.21%~43.66%)、Ms-2.1(42.36%~44.23%)、Ms-2.2(42.46%~44.15%)、Ms-2.3(43.71%~44.40%) 的 SiO₂ 含量偏高; Ms-1.1 的 Al₂O₃ 含量(34.33%~37.12%)与 Ms-1.2 的 Al₂O₃ 含量(35.17%~37.03%)相当, Ms-2.1(30.20%~34.75%)、Ms-2.2(32.47%~33.76%)、Ms-2.3(30.47%~32.55%) 的 Al₂O₃ 含量明显低于 Ms-1.1 与 Ms-1.2; Ms-1.1 的 FeO(0.42%~4.16%)、MnO(0.01%~0.15%)、MgO(0.02%~0.18%)与 Ms-1.2 的 FeO(1.41%~4.37%)、MnO(0.01%~0.07%)、MgO(0.03%~0.36%)较之 Ms-2.1 的 FeO(1.54%~5.73%)、MnO(0.11%~0.34%)、MgO(0.60%~2.68%), Ms-2.2 的 FeO(1.71%~5.76%)、MnO(0.10%~0.26%)、MgO(0.46%~2.05%), Ms-2.3 的 FeO(4.18%~6.33%)、MnO(0.10%~0.18%)、MgO(1.11%~3.34%)含量较低。根据 Tischendorf 等(1999)提出的(Fe^{tot}+Mn+Ti-Al^{VII})-(Mg-Li) 分类图对洪山沟铜金矿床中的白云母进行分类, 结果显示洪山沟铜金矿床中的白云母均为普通白云母与多硅白云母(图 7)。

根据 Miller 等(1981)提出的 Ti-Na-Mg 三角分类图解进行投图, 结果表明: Ms-1.1、Ms-1.2 全部落在原生白云母范围内, 而 Ms-2.1、Ms-2.2、Ms-2.3 落在次生白云母范围内(图 8)(Miller et al., 1981; Monier et al., 1984; 王葆华等, 2021)。

白云母 LA-ICP-MS 分析结果详见表 5, 根据 LA-ICP-MS 结果, Ms-1.1 与 Ms-1.2 相比, Ms-1.1 具有较高的 Ga(最高 20.21×10⁻⁶)、Zn(最高 190.96×10⁻⁶)、Rb(最高 227.88×10⁻⁶) 含量, Ms-1.2 具有较高的 Ba(最高 429.2×10⁻⁶)、Sn(最高 5.03×10⁻⁶)、Nb(最高 13.47×10⁻⁶)、Ti(最高 1 313.43×10⁻⁶) 含量, 二者的 Li、Zr、Cs、Cu、Sr 含量相近。

Ms-2.1 与 Ms-2.2、Ms-2.3 相比, Ms-2.1 具有较高的 W(最高 1.95×10⁻⁶)、Rb(最高 280.5×10⁻⁶)、Li(最高 309.85×10⁻⁶) 含量, Ms-2.2 具有较高的 V(最高 311.64×10⁻⁶)、Ga(最高 25.47×10⁻⁶)、Sc(最高 39.89×10⁻⁶)、Zr(最高 77.01×10⁻⁶)、Cs(最高 13.87×10⁻⁶)、Zn(最高 987.57×10⁻⁶)、Sr(最高 327.45×10⁻⁶) 含量, Ms-2.3 具有较高的 Ti(最高 1 528.64×10⁻⁶) 含量, 三者的 Sn、Cu 含量相近(图 9)。

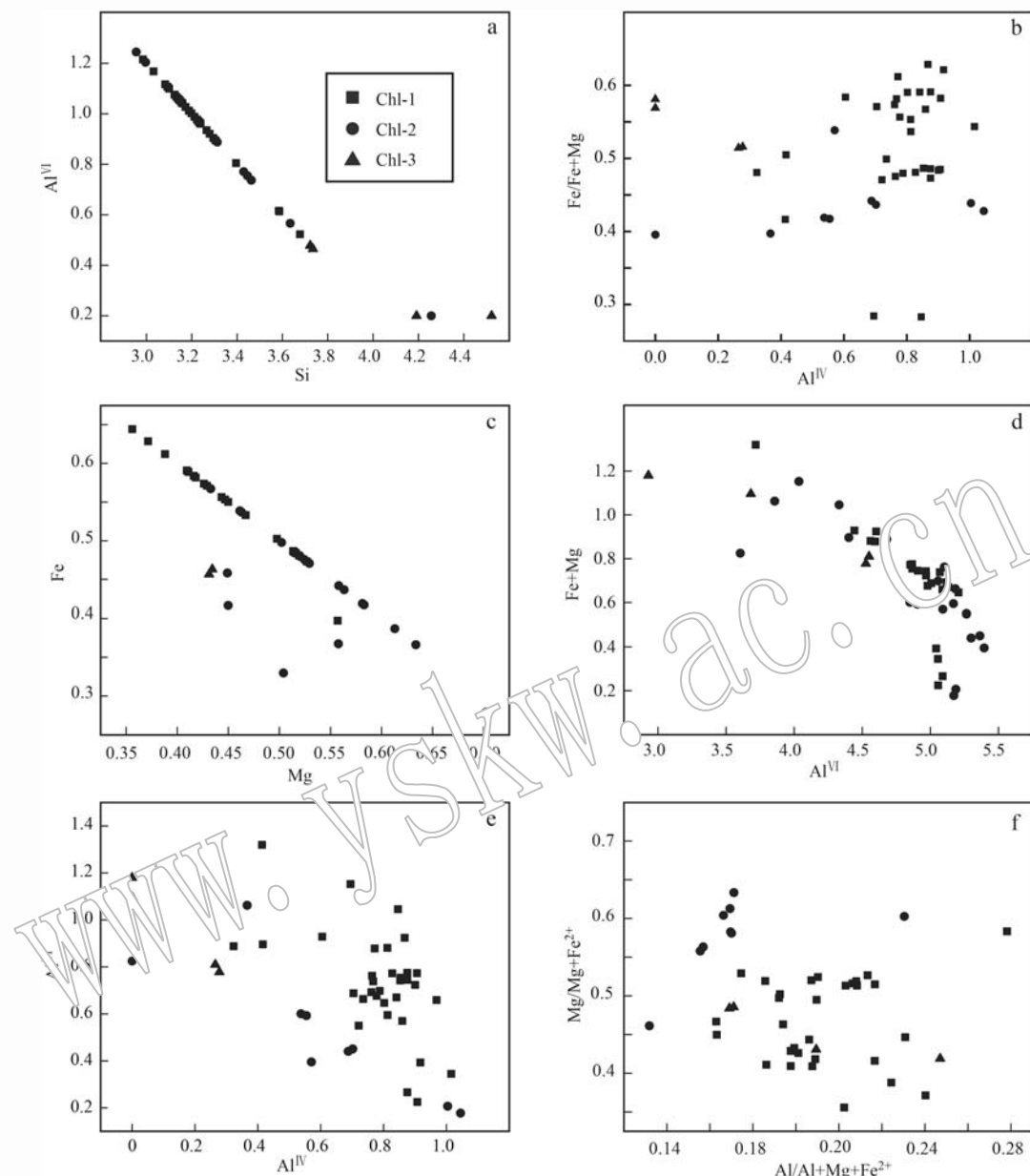


图 5 洪山沟铜金矿床中绿泥石的主要阳离子(apfu)关系图解

Fig. 5 Correlation of main cations (apfu) in chlorite from the Hongshangou copper-gold deposit

7 讨论

7.1 绿泥石形成温度

绿泥石作为中低温变质作用的产物,成分对环境极其敏感,因此可利用其成分及结构反演环境温度(Kranidiotis and Maclean, 1987; Zang and Fyfe, 1995; Zhang *et al.*, 2022)。为验证各种绿泥石地质温度计准确性,将本次地质温度计计算结果与洪山

沟铜金矿床的石英流体包裹体测温结果(125~346℃)进行对比(刘昕曜, 2016), Kranidiotis等(1987)所计算的温度与包裹体测温结果相符合,与洪山沟铜金矿床同属洪山地区的娄里金矿床(100~268℃)相近(李紫烨等, 2017)。综上,本文选择Kranidiotis等(1987)提出的地质温度计作为本文的最终结果,确定绿泥石形成温度为112~272℃之间(图10i),属于中-低温热液成矿环境,变化范围较大,推测与矿区经历多期热液活动相关(张娟等,

表 4 洪山沟铜金矿床白云母电子探针分析结果
Table 4 Electron microprobe analyses of muscovite from the Hongshangou copper-gold deposit

注：以11个氧原子为基准。

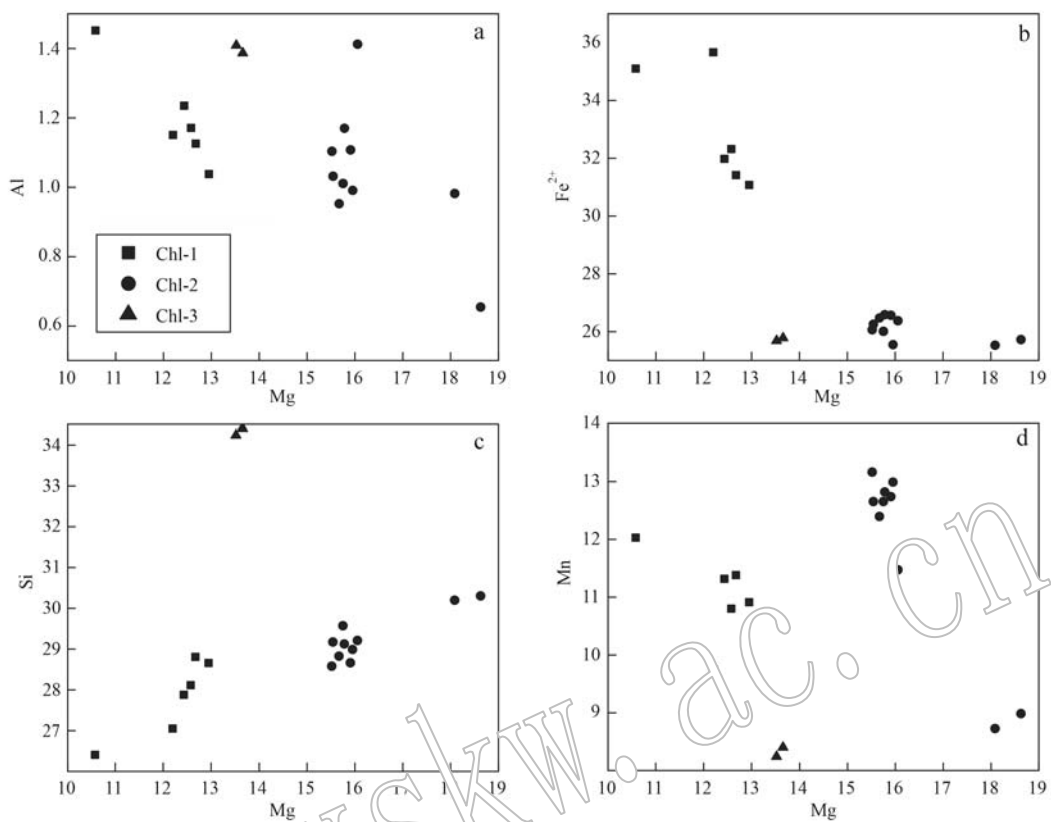


图 6 洪山沟矿床中绿泥石中主要阳离子与 Mg(apfu) 关系图解

Fig. 6 Correlation of the main cations and Mg (apfu) in chlorite in the Hongshangou deposit

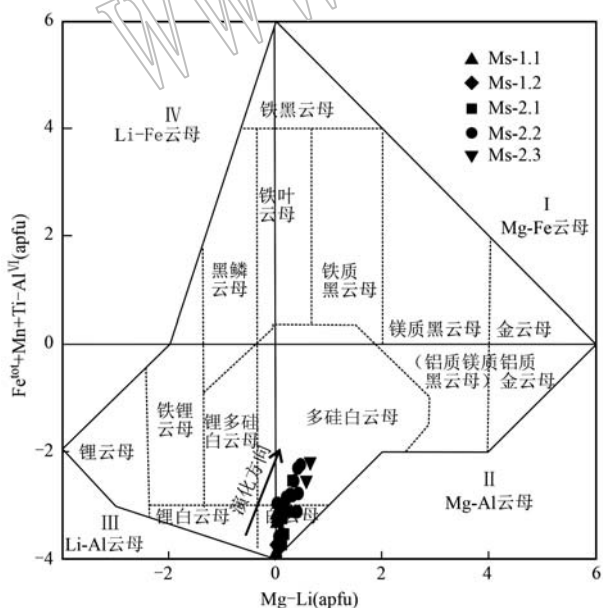
图 7 洪山沟矿床中白云母 ($\text{Fe}^{\text{tot}} + \text{Mn} + \text{Ti-Al}^{\text{VII}}$) - (Mg-Li) 分类简图 (据 Tischendorf et al., 1999)

Fig. 7 The nomenclature of the micas from the Hongshangou deposit (modified from Tischendorf et al., 1999)

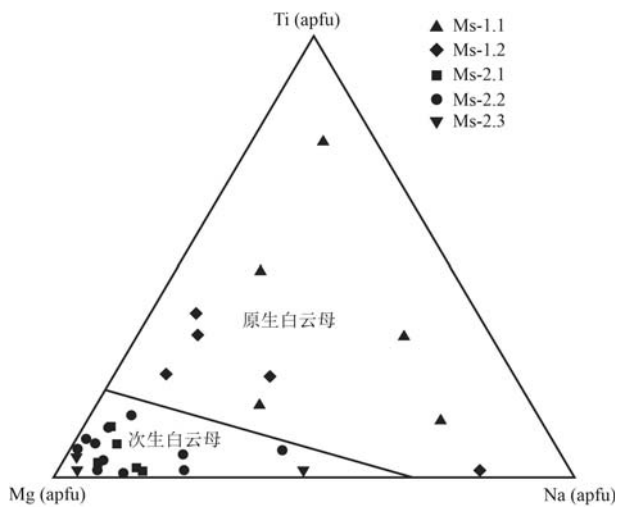


图 8 洪山沟矿床中白云母 Ti-Mg-Na 分类图

(据 Miller et al., 1981)

Fig. 8 Ti-Mg-Na ternary classification diagram of muscovite from the Hongshangou deposit (modified from Miller et al., 1981)

表 5 洪山沟铜金矿床白云母 LA-ICP-MS 分析结果
Table 5 The results of muscovite LA-ICP-MS analysis in Hongshangou copper-gold deposit

 $w_B/10^{-6}$

类型	样品号	Li	Sc	Ti	V	Cu	Zn	Ga	Rb	Sr	Zr	Nb	Sn	Cs	Ba	W
Ms-1.1	203.73-1	256.85	2.21	794.36	112.70	0.28	190.96	20.21	227.88	15.03	0.65	1.84	3.00	1.49	32.20	0.80
	203.73-2	109.41	1.85	599.37	40.45	0.24	45.86	13.23	158.61	7.45	0.11	3.25	2.82	0.47	27.59	0.40
	264.3-1	101.20	1.40	21.66	12.18	1.53	7.75	10.68	116.36	6.45	1.37	0.04	0.11	0.14	53.17	0.14
Ms-1.2	314.33-1	134.66	1.92	1008.89	67.46	0.72	14.01	10.99	197.90	11.26	0.51	12.05	5.03	0.54	334.71	0.22
	314.33-2	145.05	1.83	1313.43	59.21	1.85	15.52	11.75	214.72	8.27	0.55	13.47	4.04	0.31	429.20	0.18
	320.3-1	234.90	2.93	967.40	56.10	0.20	90.34	13.19	188.90	6.02	0.28	6.76	2.90	0.35	105.54	0.17
Ms-2.1	320.3-2	258.11	3.12	1170.53	57.91	0.32	82.59	13.50	200.44	5.92	0.28	8.16	3.25	0.40	112.58	0.17
	222.5-1	131.23	3.67	510.70	21.54	0.32	29.60	9.56	181.51	10.07	0.30	0.43	1.19	1.03	132.13	0.95
	222.5-2	243.30	3.69	1012.99	78.18	0.36	60.70	14.02	280.50	7.39	0.22	2.13	0.94	1.75	263.01	1.45
Ms-2.2	280.3-1	112.95	2.95	562.67	12.60	1.11	8.69	3.49	169.10	35.07	0.47	0.74	1.11	0.31	482.85	0.76
	280.3-2	228.40	3.32	853.86	23.78	9.31	61.72	7.35	270.59	35.18	2.43	2.43	1.12	1.27	258.16	1.95
	364-2	309.85	2.98	31.15	5.08	0.16	18.81	10.82	196.86	68.34	0.65	0.40	1.13	0.53	5.44	0.21
Ms-2.2	203.73-1	294.36	2.08	1314.74	64.22	0.19	43.70	14.14	190.19	27.33	8.72	19.57	5.03	0.43	48.19	0.38
	264.3-2	130.75	32.53	976.78	252.96	1.79	779.22	24.87	176.88	30.13	77.01	0.32	5.90	1.49	14.43	0.20
	416.1-1	122.20	39.89	515.72	311.64	0.83	987.57	25.47	183.18	109.72	45.57	0.75	10.76	9.36	7.14	0.03
Ms-2.3	416.1-2	123.00	16.32	493.08	121.53	2.26	624.13	20.46	309.03	327.45	1.83	0.48	1.38	13.77	29.09	0.08
	416.1-3	20.23	3.40	169.79	129.07	18.84	3.91	10.76	33.88	151.03	1.96	3.23	3.15	0.26	99.60	1.20
	264.3-3	106.90	2.72	327.40	74.74	1.85	76.65	13.82	175.15	7.9	1.18	3.73	0.46	0.41	83.32	0.22
Ms-2.3	320.3-1	122.18	3.59	1144.43	74.96	0.63	133.69	13.24	216.65	1.79	0.1	2.46	3.37	0.30	91.57	0.07
	320.3-2	116.16	4.09	1528.64	84.20	0.67	139.16	15.42	241.47	1.16	0.27	2.63	4.95	0.36	92.69	0.12

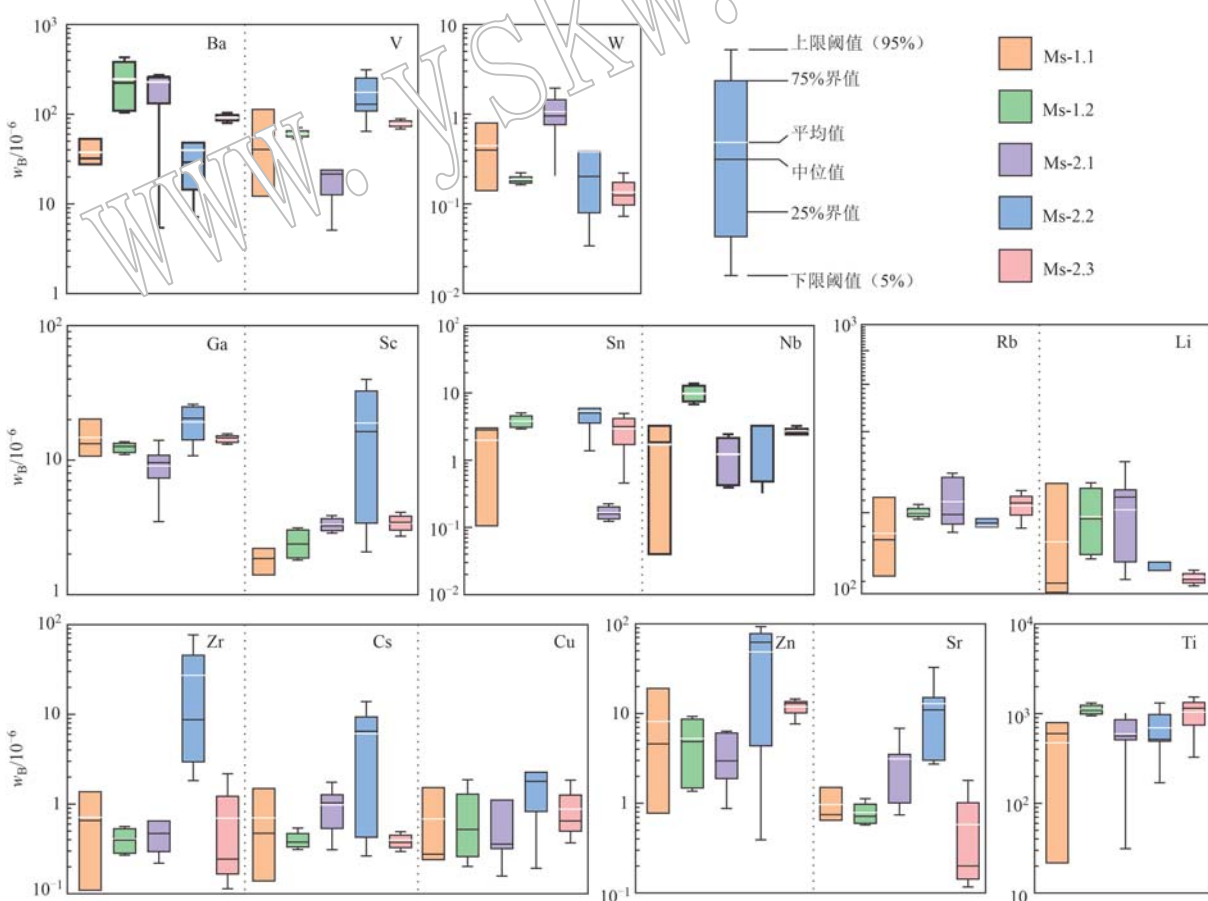


图 9 洪山沟铜金矿床各类型白云母微量元素成分箱状图

Fig. 9 Box diagrams of trace element composition of various types of muscovite in Hongshangou copper-gold deposit

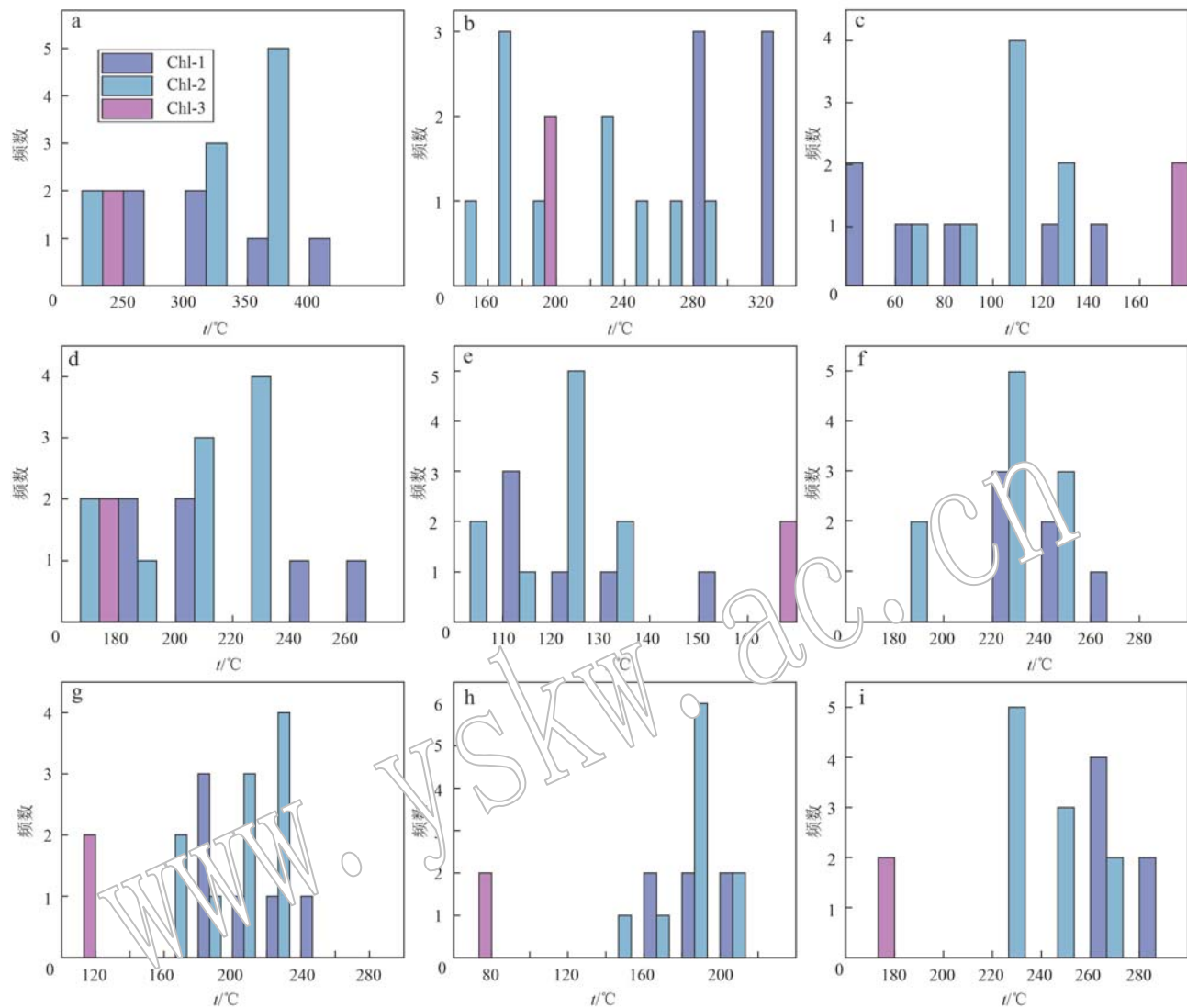


图 10 洪山沟矿床中绿泥石温度直方图

Fig. 10 Histograms showing the temperature of chlorite in the Hongshangou deposit

2021)。前人所做流体包裹体结果证明洪山沟铜矿成矿流体绝大部分测温结果集中于210~310℃之间且晚期有大气水加入(刘昕曜, 2016), 铜沉淀的温度一般在250~350℃之间, 其中Chl-1峰值比较集中, 在242~280℃之间, Chl-2较为分散, 在197~246℃之间, 说明各绿泥石形成于各成矿阶段的晚期。推测成矿早期流体温度较高, 随着流体运移, 浅部大气降水与深部岩浆热液的流体混合导致成矿温度、压力逐渐下降, 进而导致隐爆作用的产生; 而大气降水的参与也使得流体pH值升高并偏于中性热液的溶解度降低, 导致金属硫化物析出沉淀。前人研究认为, 100~350℃内温度与绿泥石Al^{IV}值呈正相关关系, 而与八面体空位和Al^{VII}呈负相关关系

(Cathelineau and Nieva, 1985; Cathelineau, 1988)。洪山沟铜金矿床中的绿泥石形成温度与Al^{IV}、Si均呈较好的线性相关关系(图11), 该结果与前人研究成果相似, 证实了该温度体系的适用性(周栋等, 2018; 葛祥坤等, 2020; 张娟等, 2021; 刘松岩等, 2024)。

7.2 绿泥石形成环境

洪山沟铜金矿床中铜金矿均赋存于霓辉正长斑岩中, 且富矿的正长斑岩中绿泥石化较为发育, 可见明显的绿泥石交代作用, 热液侵入, 导致原岩中角闪石、黑云母发生蚀变交代, 从而形成大量的蚀变绿泥石。前人研究证明绿泥石成分中Fe²⁺与Mg²⁺会发生广泛的类质同象取代(艾永富等, 1998; Chu *et al.*,

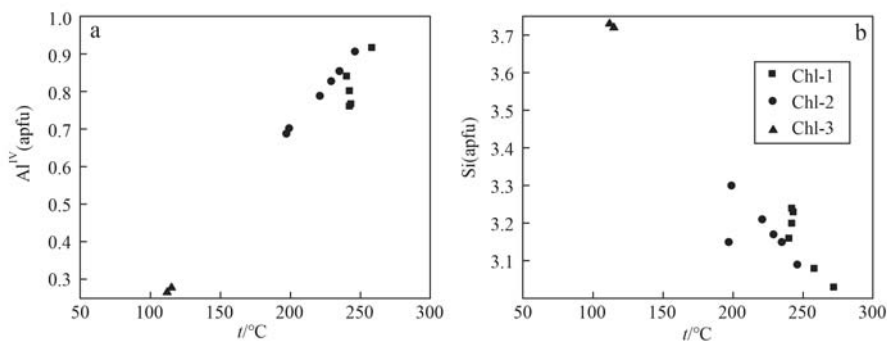


图 11 洪山沟矿床中绿泥石形成温度与 Si 、 Al^{IV} 相关性图解
Fig. 11 Correlation of Si , Al^{IV} with temperature of chlorites in the Hongshangou deposit

2020), 在斑岩型矿床中, Fe 绿泥石倾向于在高温环境中形成, 随着温度降低与 pH 值升高, 导致绿泥石中出现 Fe 、 Mg 置换, 大量 Mg^{2+} 进入绿泥石晶格, 形成 Mg 绿泥石, 本次研究采用 Zane 等(1998)限定绿泥石结构类型和八面体占位主导阳离子的三角分类图解, 对洪山沟铜金矿床中绿泥石进行分类。据图 12 可知, 洪山沟铜金矿床中绿泥石均属三八面体 type-I 型绿泥石, 八面体中 Fe^{2+} 占主导地位, 为 Fe 绿泥石, 指示洪山沟铜金矿床中的绿泥石形成于还原环境。在温度条件相近的中温热液矿床形成过程中, 溶液的酸碱度对绿泥石成分有明显影响, 前人证明 $\text{Fe}/(\text{Fe}+\text{Mg})$ 值可反映绿泥石结晶时所处环境。一般认为 $\text{Fe}/(\text{Fe}+\text{Mg}) > 0.5$, 更易形成 Fe 绿泥石。洪山沟

铜金矿床中 Chl-1 的 $\text{Fe}/(\text{Fe}+\text{Mg})$ 值为 0.57~0.65 (均值为 0.60), Chl-2 的 $\text{Fe}/(\text{Fe}+\text{Mg})$ 值为 0.44~0.49 (均值为 0.47), Chl-3 的 $\text{Fe}/(\text{Fe}+\text{Mg})$ 值为 0.51~0.52 (均值为 0.51), 指示绿泥石形成经历了流体还原性-近中性的演化过程, 黄铜矿沉淀于近还原性的环境。斑岩型矿床的含矿热液具氧化性, 赋存大量矿床(Sun et al., 2013, 2015; 贺文等, 2023), 在洪山沟成矿过程中, 热液向上运移蚀变侵入岩, 铁镁质矿物中的 Fe^{2+} 进入热液, 中和热液的氧化性, 导致金属硫化物沉淀, 此时成矿流体为近中性环境, 证明洪山沟铜金矿床成矿环境由氧化性到近还原性的转变。流体性质差异及成矿环境对金成矿起到抑制作用, 导致洪山沟铜金矿床中金见矿效果较差。

7.3 绿泥石微量元素对矿床的指示

已有众多学者证明绿泥石微量元素能够作为斑岩型矿床的勘查矢量工具(Jago et al., 2014; Pacey et al., 2020; Xue et al., 2021)。Wilkinson 等(2015)研究 Batu Hijau 矿床时发现绿泥石化学与斑岩热液中心呈系统性变化, 特别是在距斑岩 2.5 km 半径范围内, 随着距离的增加青磐岩化绿泥石中 Ti、V 等离子浓度呈指数级下降, 而 Li、Sr、Ba、Mn、Co、Ni、Zn 和 Pb 浓度呈指数级上升, 并提出 Ti 在斑岩系统中绿泥石元素空间变化规律可能与两种机制有关: ① 与热液流体的迁移扩散有关, 如斑岩矿床矿体外围经常出现的贵、贱金属异常; ② 由温度控制的元素替换。国内外众多学者对绿泥石微量元素的研究表明, 由于矿床不同形成环境, Zn、Mn、Sc、Sr、Li 与温度呈正相关性或负相关性, 但都证明了 Ti、V 会随着远离热液矿化中心逐渐降低(Xiao et al., 2018; Xiao and Chen, 2020)。据绿泥石微量元素箱状图(图 13)可看出, 洪山沟矿床中完全蚀变的绿泥石

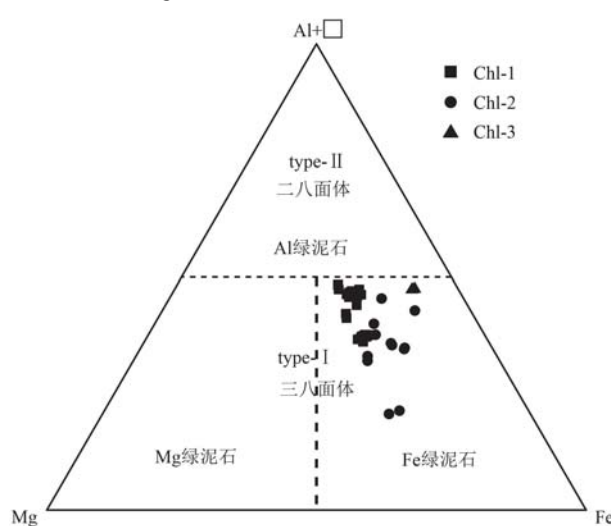


图 12 洪山沟矿床中绿泥石分类图解(底图据 Zane and Weiss, 1998)
Fig. 12 Classification diagram for chlorite from the Hongshangou deposit (base map after Zane and Weiss, 1998)

Fig. 12 Classification diagram for chlorite from the Hongshangou deposit (base map after Zane and Weiss, 1998)

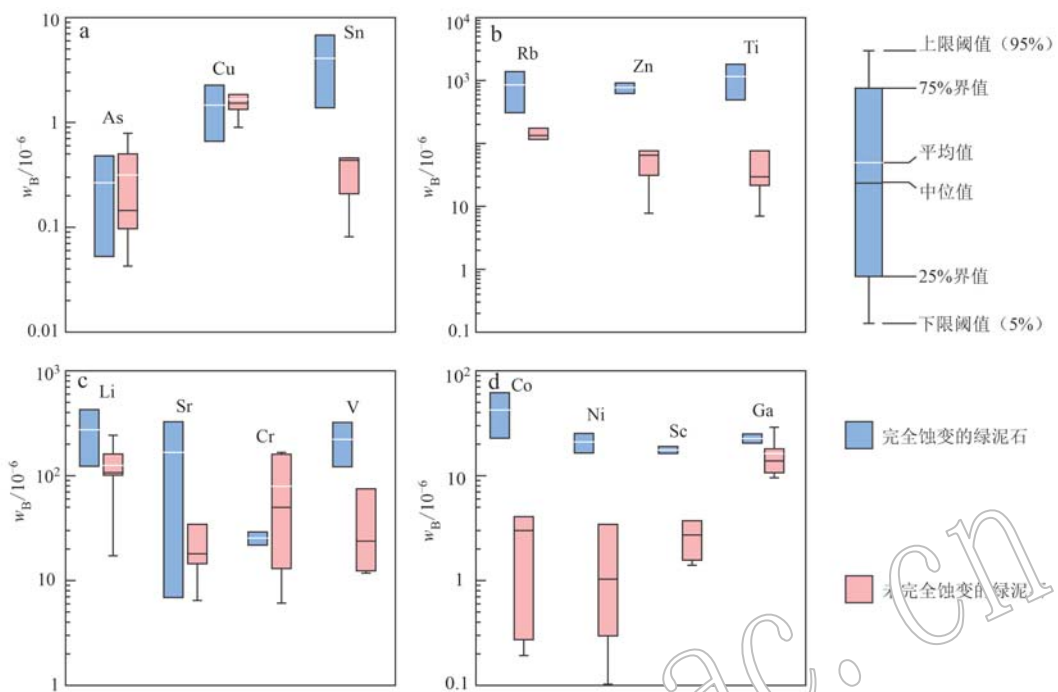


图 13 洪山沟铜金矿床各类型绿泥石微量元素成分箱状图

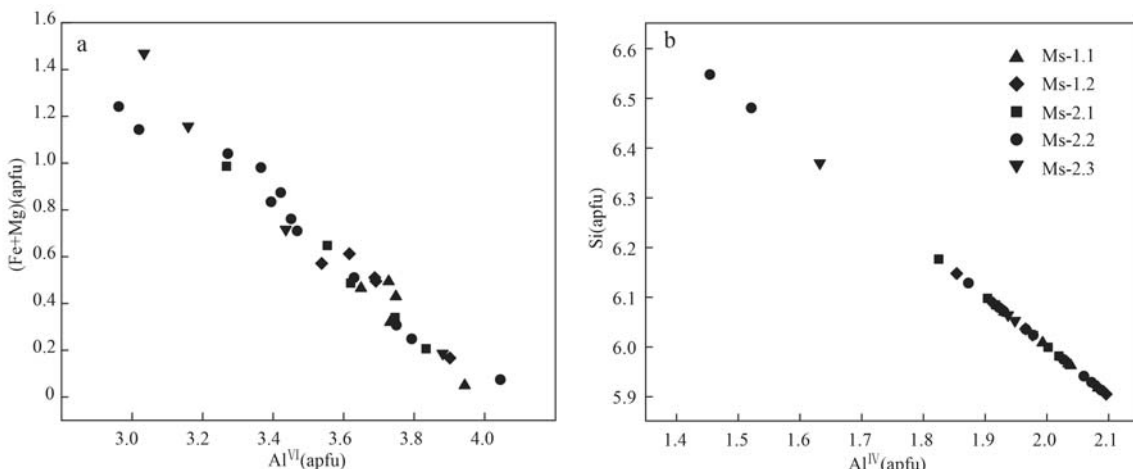
Fig. 13 Box diagrams of trace element composition of various types of chlorite in Hongshangou copper-gold deposit

中,Sn、Rb、Zn、Ti、V、Co、Ni、Sc 的含量均明显高于未完全蚀变的绿泥石,完全蚀变的绿泥石比未完全蚀变的绿泥石的深度要深。尽管本次研究中绿泥石微量元素样品较少,但微量元素变化趋势明显,推测洪山沟铜金矿床的矿化热液中心还在深部。

7.4 白云母形成环境

白云母是含水层状硅酸盐矿物,常见于热液蚀变环境,其形成受热液性质(成分、温度、压力、pH 值等)、围岩性质及水/岩比例等因素影响(Guidotti *et al.*, 1994; Duke, 1994; Halley *et al.*, 2015; 郭娜

等, 2017; 贺文等, 2023)。洪山沟铜金矿床中,白云母与多硅白云母共存。电子探针结果显示,白云母八面体位置发生 Fe、Mg 对 Al^{VI}的置换,四面体位置存在 Si 对 Al^{IV}的置换(图 14)。多硅白云母与矿化关系密切,而无矿岩体中主要为普通白云母。深部流体富含 CO₂,水解后呈酸性,促进水岩反应,形成高 Al 低 Si 的白云母;随着流体上移,Fe²⁺进入降低氧化性,pH 值升高,导致 Fe、Mg 置换 Al^{VI}及 Si 置换 Al^{IV},形成高 Si 低 Al 的多硅白云母,Cu 随之沉淀成矿。

图 14 白云母(Fe+Mg)与 Al^{VI}(a)和 Si 与 Al^{IV}(b)的关系图Fig. 14 Correlation of the (Fe+ Mg) and Al^{VI}(a), Si and Al^{IV}(b) of muscovite

多硅白云母是变质和热液交代作用的产物,可在低压低温及中压低温环境下稳定存在(叶美芳等,2016)。洪山沟矿床中Cu在中低温-近中性环境下沉淀,金属硫化物更倾向于在此条件下沉淀(Hemley and Jones, 1964; Portela *et al.*, 2021)。随着流体上移,Fe²⁺降低氧化性,流体近中性,金属硫化物开始沉淀(Li *et al.*, 2013),pH值升高促使Fe、Mg置换Al^{VI}及Si置换Al^{IV},形成富Si贫Al的白云母。

洪山沟矿床白云母微量元素差异显著。原生白云母Ms-1.1、Ms-1.2中Li、Zr、Cs、Cu、Sr含量接近,次生白云母Ms-2.1、Ms-2.2、Ms-2.3中Sn、Cu含量接近,V、W、Sc、Zn、Ti在次生白云母中富集。V、Sc差异反映白云母形成时期(Uribe-Mogollon and Maher, 2018, 2020),Ti、V、W、Sn等高价元素在高氧化条件下不易进入云母晶格,Sc在高氧逸度下更易进入磁铁矿或赤铁矿,早期云母亏损V、Sc,晚期云母富集V、Sc。Ms-2.1的V、Sc含量高于Ms-2.2、Ms-2.3。Zn在高温蚀变中不易进入云母晶格,高温中心云母具低Cu、Zn特征(Chaffee, 1982; Hailey

et al., 2015)。Ms-2.3的Zn含量低于Ms-2.1、Ms-2.2,表明其形成于早期高温蚀变,Ms-2.1、Ms-2.2形成于成矿中晚期。

白云母微量元素相关性图解(图15)显示,微量元素变化反映白云母共生阶段、围岩和流体组成、pH值、压力、温度条件及其沉淀相元素分配(Ayuso, 1987; Loucks, 2014; Benavides, 2017; Alva-Jimenez *et al.*, 2020)。Ms-2.3较Ms-2.1、Ms-2.2富集Sn,亏损V、W、Zn,表明其形成于早期低pH值、氧化性条件(Mallmann and O'Neill, 2013)。综上,洪山沟矿床成矿流体早期具高氧逸度、低pH值特征,Ms-2.3伴随少量矿化形成;后期富Sc、V的Ms-2.1形成,表明成矿流体后期有大气降水加入,热液温度与氧逸度降低。

7.5 流体演化及成矿指示意义

斑岩型矿床中,矿化中心的成矿流体具高温高氧化特征,向外渐水岩反应导致岩浆中的硫酸盐矿物发生还原反应生成氧化性的含铁矿物(Ohmoto, 1997)。在洪山沟铜金矿床成矿过程中,与白云母共生

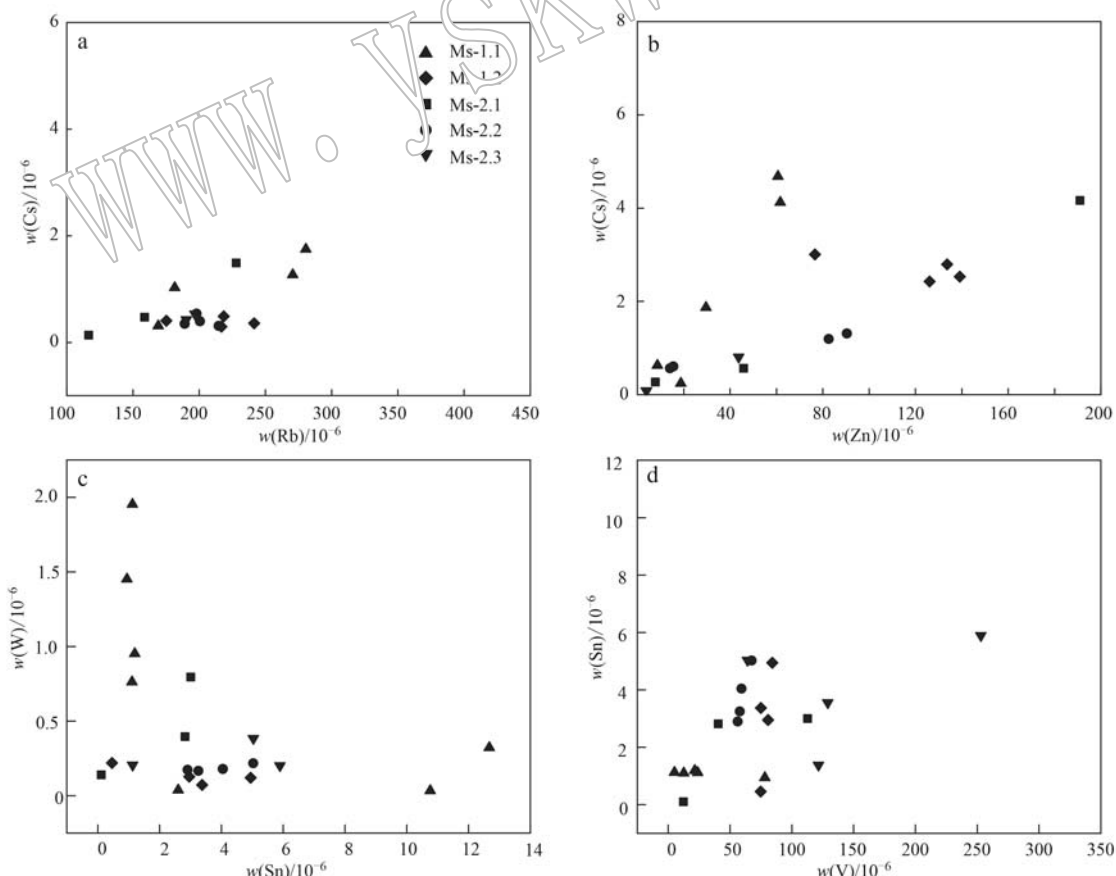


图15 洪山沟铜金矿床白云母微量元素二元图解

Fig. 15 Binary diagrams of muscovite trace elements in Hongshangou copper-gold deposit

的方解石指示在成矿初期流体富含 CO_2 , 流体呈酸性, 温度较高抑制白云母离子间发生契尔马克置换(唐楠等, 2021; 田成华等, 2022), 此时白云母为富 Al 贫 Si 的白云母, Cu 与 Cl 形成氯络合物进行运移, 随着大气水的加入, 流体温度下降, 高温钾化蚀变逐渐向低温绢云母化、青磐岩化蚀变发展, Fe^{2+} 进入流体使流体从氧化性向中性转变, Cu 开始沉淀并富集成矿(杨航等, 2023; 李发桥等, 2024), 与矿物共生的绿泥石 Chl-1 的形成温度为 270~280°C, 此时流体温度降低, pH 值升高, 白云母为高 Si 低 Al 的多硅白云母, 表明洪山沟铜金矿床主要成矿环境为中-低温近中性环境。

8 结论

(1) 洪山沟铜金矿床中 3 类绿泥石形成温度在 112~272°C 之间, 其中与金属矿物共(伴)生的绿泥石温度在 242~272°C 之间, 微量元素指示洪山沟铜金矿床形成于中-低温热液成矿环境;

(2) 绿泥石微量元素结果表明完全蚀变的绿泥石更富 Sn、Rb、Zn、Ti、V、Co、Ni、Sc, 暗示深部还有热源的可能;

(3) 洪山沟铜金矿床中与长石共生的片状白云母、与方解石共生片状白云母为岩浆演化形成的普通白云母。与长石共生细小鳞片状白云母, 与长石、黄铜矿共生的片状白云母以及与方解石、黄铜矿共生鳞片状-片状白云母为热液蚀变形成的多硅白云母。与矿化密切相关的白云母具高 Si、Fe、V、W 低 Al、Sn 的特征, 指示洪山沟铜金矿床成矿流体早期呈酸性, 氧逸度较高, 后期随着大气降水的加入导致流体逐渐向中性转变, 氧逸度降低。表明洪山沟铜金矿床成矿环境为近中性环境。

References

- Adegoke I A, Xia F, Deditius A P, et al. 2022. A new mode of mineral replacement reactions involving the synergy between fluid-induced solid-state diffusion and dissolution-reprecipitation: A case study of the replacement of bornite by copper sulfides [J]. *Geochimica et Cosmochimica Acta*, 330: 165~190.
- Ai Yongfu and Liu Guoping. 1998. The study of chlorite at Dajing deposit in Inner-Mongolia of China [J]. *Acta Scientiarum Naturalium Universitatis Pekinensis*, 34(1): 99~107 (in Chinese with English abstract).
- Alva-Jimenez T, Tosdal R M, Dilles J H, et al. 2020. Chemical variations in hydrothermal white mica across the Highland Valley porphyry Cu-Mo district, British Columbia, Canada [J]. *Economic Geology*, 115(4): 903~926.
- Ayuso R A. 1987. White Mica Geochemistry of the Catheart Mountain Porphyry Copper Deposit, Maine [R]. US Government Printing Office.
- Bai Fusheng. 2022. Study on the Genesis and Mineralization of Hongshan Complex in Han-Xing Area, Southern Hebei Province [D]. Shijiazhuang: Hebei Geology University (in Chinese with English abstract).
- Basori M B I, Zaw K, McNeill A, et al. 2022. A mineralogical and geochemical application for determining hydrothermal alteration zones associated with volcanic-hosted massive sulphide deposits at Tasik Chinini area, Peninsular Malaysia [J]. *Applied Geochemistry*, 145(2): 105~104.
- Battaglia S. 1990. Applying X-ray geothermometer diffraction to a chlorite [J]. *Clay and Clay Minerals*, 47(1): 54~63.
- Ba David S B. 2017. Characterisation of Sericitic Alteration at the Tacabajo Porphyry Cu Deposit, Argentina [D]. University of Tasmania.
- Bryndzia L T and Scott S D. 1987. The composition of chlorite as a function of sulfur and oxygen fugacity: An experimental study [J]. *American Journal of Science*, 287(1): 50~76.
- Cathelineau M. 1988. Cation site occupancy in chlorites and illites as a function of temperature [J]. *Clay Minerals*, 23(4): 471~485.
- Cathelineau M and Nieva D. 1985. A chlorite solid solution geothermometer the Los Azufres (Mexico) geothermal system [J]. *Contributions to Mineralogy and Petrology*, 91(3): 235~244.
- Cerný P, Chapman R, Teerstra D K, et al. 2003. Rubidium and cesium dominant micas in granitic pegmatites [J]. *American Mineralogist*, 88(12): 1832~1835.
- Chaffee M A. 1982. A geochemical study of the Kalamazoo porphyry copper deposit, Pinal County, Arizona [J]. *Advances in Geology of the Porphyry Copper Deposits*; Titley, SR, Ed: 211~225.
- Chang Hao, Zhang Liangliang and Yue Peng. 2020. Preliminary study on geological characteristics and genesis of Hongshangou copper deposit in Handan City [J]. *China Metal Bulletin*, (1): 37, 39 (in Chinese with English abstract).
- Chang Hao, Zhang Liangliang, Yue Peng, et al. 2017. Preliminary Survey Report on the Hongshangou Copper and Polymetallic Deposit in Wu'an City, Hebei Province [R]. Ninth Geology Division of Hebei Bureau of Geology and Mineral Resources Exploration (in Chinese).
- Chang J, Li J W and Audébat A. 2018. Formation and evolution of multi-

- stage magmatic-hydrothermal fluids at the Yulong porphyry Cu-Mo deposit, eastern Tibet: Insights from LA-ICP-MS analysis of fluid inclusions[J]. *Geochimica et Cosmochimica Acta*, 232: 181~205.
- Chen Yanjing, Ni Pei, Fan Hongrui, et al. 2007. Diagnostic fluid inclusions of different types hydrothermal gold deposits[J]. *Acta Petrologica Sinica*, 23 (9): 2 085~2108 (in Chinese with English abstract).
- Chu G, Zhang S, Zhang X, et al. 2020. Chlorite chemistry of Tongshankou porphyry-related Cu-Mo-W skarn deposit, Eastern China: Implications for hydrothermal fluid evolution and exploration vectoring to concealed orebodies[J]. *Ore Geology Reviews*, 122: 103531.
- Chu Xiangkai, Shen Ping, Li Changhao, et al. 2023. Ore-forming fluid evolution of the Wunugetushan porphyry Cu-Mo deposit, Inner Mongolia: Evidence from the short-wave infrared spectrum, mica composition and fluid inclusion of quartz[J]. *Acta Petrologica Sinica*, 39 (11): 3 461~3 478 (in Chinese with English abstract).
- Cui Xiaoliang, Su Shangguo, Zhang Yanan, et al. 2022. Deep magmatic process of the Fushan complex in the southern section of Taihang Mountain, Hebei Province and its tectonic significance[J]. *Earth Science Frontiers*, 29(1): 342~363 (in Chinese with English abstract).
- Duke E F. 1994. Near infrared spectra of muscovite, scherlak substitution, and metasomatic reaction processes: Implications for remote sensing[J]. *Geology*, 22(7): 621~624.
- Feng Y, Chu G, Xie B, et al. 2022. Chlorite mineralogy, geochemistry and exploration implications: A case study of the Xiaokelehe porphyry Cu-Mo deposit in NE China[J]. *Ore Geology Reviews*, 140: 104~568.
- Fu Jiangang, Li Guangming, Guo Weikang, et al. 2023. Mineral geochemical characteristics of muscovite and its implication for rare metal mineralization in leucogranites in the Lalong Dome, Xizang, China [J]. *Journal of East China University of Technology (Natural Science)*, 46(6): 555~575 (in Chinese with English abstract).
- Ge Xiangkun, Ju Haiyu, Zhao Fenghua, et al. 2020. Characteristics of chlorites in the Shangdajing porphyry Mo deposit, Inner Mongolia and their metallogenetic implications [J]. *Geology and Exploration*, 56 (4): 704~713 (in Chinese with English abstract).
- Geng Guojian, Ma Baojun and Shen Fangle. 2023. Geological characteristics and mineralization of Taoyuan copper deposit in south part of Taihang Mountain[J]. *Journal of Hebei GEO University*, 46(4): 90~100 (in Chinese with English abstract).
- Guidotti C V, Sassi F P, Blencoe J G, et al. 1994. The paragonite-muscovite solvus: I. PTX limits derived from the Na-K compositions of natural, quasibinary paragonite muscovite pairs [J]. *Geochimica et Cosmochimica Acta*, 58(10): 2 269~2 275.
- Guo Guolin, Liu Xiaodong, Pan Jiayong, et al. 2012. Character of chlorite and its relationship to uranium mineralization in uranium deposit No. 302[J]. *Uranium Geology*, 28(1): 35~41 (in Chinese with English abstract).
- Guo Na, Huang Yiru, Zheng Long, et al. 2017. Alteration zoning and prospecting model of epithermal deposit revealed by shortwave infrared technique: A case study of Tiegelongnan and Sinongduo Deposits [J]. *Acta Geoscientica Sinica*, 38(5): 767~778 (in Chinese with English abstract).
- Halley S, Dilles J H and Tosdal R M. 2015. Footprints: Hydrothermal alteration and geochemical dispersion around porphyry copper deposits [J]. *SEG Newsletter*, 100(1): 1~17.
- He Wen, Lin Bin, Song Yingxin, et al. 2023. Mineralogical characteristics and implications of muscovite from the Tiegelongnan super-large copper (gold) deposit in Tibet[J]. *Acta Geologica Sinica*, 97(6): 1 938~1 945 (in Chinese with English abstract).
- Haley J and Jones W R. 1964. Chemical aspects of hydrothermal alteration with emphasis on hydrogen metasomatism[J]. *Economic Geology*, 59(4): 538~569.
- Hillier S. 1993. Origin, diagenesis, and mineralogy of chlorite minerals in Devonian lacustrine mudrocks, Orcadian Basin, Scotland [J]. *Clays and Clay Minerals*, 41(2): 240~259.
- Hiller S and Velde B. 1991. Octahedral occupancy and the chemical composition of diagenetic (low-temperature) chlorites[J]. *Clay Minerals*, 26: 149~168.
- Hou Zengqian, Pan Xiaofei, Yang Zhiming, et al. 2007. Porphyry Cu-(Mo-Au) deposits no related to oceanic-slab subduction: Examples from Chinese porphyry deposits in continental settings[J]. *Geoscience*, 21(2): 332~351 (in Chinese with English abstract).
- Hou Z Q, Yang Z M, Lü Y J, et al. 2015. A genetic linkage between subduction and collision-related porphyry Cu deposits in continental collision zones[J]. *Geology*, 43(3): 247~250.
- Inoue A. 1952. Formation of Clay Minerals in Hydrothermal Environments Veide. *Origin and Mineralogy of Clays*[M]. Berlin: Springer, 268~330.
- Inoue A. 1995. Formation of clay minerals in hydrothermal environments [J]. *Origin and Mineralogy of Clays: Clays and the Environment*, 268~329.
- Inoue A, Meunier A, Patrier M P, et al. 2009. Application of chemical geothermometry to low-temperature trioctahedral chlorites[J]. *Clays and Clay Minerals*, 57(3): 371~382.

- Jago C P, Tosdal R M, Cooke D R, et al. 2014. Vertical and lateral variation of mineralogy and chemistry in the Early Jurassic Mt. Milligan alkalic porphyry Au-Cu deposit, British Columbia, Canada [J]. *Economic Geology*, 109(4): 1 005~1 033.
- Jowett E C. 1991. Fitting iron and magnesium into the hydrothermal chlorite geothermometer: Program with abstracts[J]. *Geological Association of Canada*, 16: 62.
- Kavalieris I, Walshe J L, Halley S, et al. 1990. Dome-related gold mineralization in the Pani volcanic complex, North Sulawesi, Indonesia; A study of geologic relations, fluid inclusions, and chlorite compositions[J]. *Economic Geology*, 85(6): 1 208~1 225.
- Keppler H. 1993. Influence of fluorine on the enrichment of high field strength trace elements in granitic rocks[J]. *Contributions to Mineralogy and Petrology*, 114: 479~488.
- Kranidiotis P and MacLean W H. 1987. Systematics of chlorite alteration at the Phelps Dodge massive sulfide deposit, Matagami, Quebec[J]. *Economic Geology*, 82(7): 1 898~1 911.
- Laakso K, Peter J M, Rivard B, et al. 2016. Short-wave infrared spectral and geochemical characteristics of hydrothermal alteration at the Archean Izok Lake Zn-Cu-Pb-Ag volcanogenic massive sulfide deposit, Nunavut, Canada: Application in exploration target vectoring[J]. *Economic Geology*, 111(5): 1 223~1 239.
- Laird J. 1988. Chlorites. Metamorphic petrology[J]. *Reviews in Mineralogy*, 19(1): 405~421.
- Legros H, Marignac C, Tabary T, et al. 2018. The ore forming magmatic-hydrothermal system of the Piaotang W-Sn deposit (Jiangxi, China) as seen from Li-mica geochemistry[J]. *American Mineralogist*, 103(1): 39~54.
- Li C, Shen P, Zhao Y, et al. 2022. Mineral chemistry of chlorite in different geologic environments and its implications for porphyry Cu±Au±Mo deposits[J]. *Ore Geology Reviews*, 149: 105~112.
- Li Faqiao, Tang Juxing, Song Yang, et al., 2024. Mineralogical characteristics and geological significance of apatite in the Naruo porphyry Cu (Au) deposit in Duolong ore district, northwestern Xizang (Tibet)[J]. *Geological Review*, 70(3): 885~906 (in Chinese with English abstract).
- Li J, Huang X L, He P L, et al. 2015. In situ analyses of micas in the Yashan granite, South China: Constraints on magmatic and hydrothermal evolutions of W and Ta-Nb bearing granites[J]. *Ore Geology Reviews*, 65(4): 793~810.
- Li Jinwen, Zhang Dequan, Zhao Shibao, et al. 2006. Metallogenic regularity and prospecting targets in the southwest part of the Derbugan metallogenic belt[J]. *Mineral Deposits*, 25(S1): 19~22 (in Chinese with English abstract).
- Li Suimin, Li Yucheng, Zhao Shumei, et al. 2022. Ar-Ar and U-Pb ages of Hongshan copper deposit, Handan City, Hebei Province and their limitation on mineralization age[J]. *Geology in China*, 49(2): 575~585 (in Chinese with English abstract).
- Li Yucheng, Jia Liqin, Zhao Shumei, et al. 2016. Lithographic characteristics of Hongshan volcanic edifice in the southern section of Taihang Mountains[J]. *Modern Mining*, 32(5): 142~145 (in Chinese with English abstract).
- Li Z K, Li J W, Zhao X F, et al. 2013. Crustal extension Ag-Pb-Zn veins in the Xiong'ershan District, Southern North China craton: Constraints from the Shagou deposit[J]. *Economic Geology*, 108(7): 1 703~1 729.
- Li Ziye, Xing Huan, Li Suimin, et al. 2017. Fluid inclusions test of Louli gold deposit and their geological significance[J]. *Contributions to Geology and Mineral Resources Research*, 32(2): 205~213 (in Chinese with English abstract).
- Liu Songyan, Zhang Da, Yang Mingjian, et al. 2024. Characteristics of chlorites from the Haopinggou Ag-Au polymetallic deposit in the Xiong'ershan ore concentration area and its exploration implications [J]. *Journal of Geomechanics*, 30(1): 129~146 (in Chinese with English abstract).
- Liu Xinyao. 2016. Petrogenesis and Metallogenesis of Hongshan Orthophyre in Southern Taihang Mountain [D]. China University of Geosciences (in Chinese with English abstract).
- Loucks R R. 2014. Distinctive composition of copper ore forming arcmagmas[J]. *Australian Journal of Earth Sciences*, 61(1): 5~16.
- Ma Wanwei, Huang Xiaolong, Yu Yang, et al. 2020. Characteristics of micas in the Limu granites, South China: An indicator of the hydrothermal processes related to tin mineralization[J]. *Geotectonica et Metallogenesis*, 44(6): 1 143~1 159 (in Chinese with English abstract).
- Mallmann G and O'Neill H S C. 2013. Calibration of an empirical thermometer and oxybarometer based on the partitioning of Sc, Y and V between olivine and silicate melt[J]. *Journal of Petrology*, 54(5): 933~949.
- Mernagh T P, Leys C and Henley R W. 2020. Fluid inclusion systematics in porphyry copper deposits: The super-giant Grasberg deposit, Indonesia, as a case study[J]. *Ore Geology Reviews*, 123: 103~1570.
- Miller C F, Stoddard E F, Bradfish L J, et al. 1981. Composition of plutonic muscovite: Genetic implications[J]. *Canadian Mineralogist*, 19(1): 25~34.
- Monier G, Mergoil D J and Labernadière H. 1984. Générations successives de muscovites et feldspaths potassiques dans les leucogranites

- du massif de Millevaches (Massif Central Français) [J]. *Bulletin de Minéralogie*, 107(1): 55~68.
- Neiva A M R. 2013. Micas, feldspars and columbite-tantalite minerals from the zoned granitic lepidolite-subtype pegmatite at Namivo, Alto Ligonha, Mozambique[J]. *European Journal of Mineralogy*, 25(6): 967~985.
- Ohmoto H. 1997. Applications of sulfur and carbon isotopes in ore deposit research[J]. *Geochemistry of Hydrothermal Ore Deposits*, 517~611.
- Pacey A, Wilkinson J J and Cooke D R. 2020. Chlorite and epidote mineral chemistry in porphyry ore systems: A case study of the North-parkes district, New South Wales, Australia[J]. *Economic Geology*, 115(4): 701~727.
- Pak S J, Choi S G and Choi S H. 2004. Systematic mineralogy and chemistry of gold silver vein deposits in the Taebaeksan district, Korea: Distal relatives of a porphyry system[J]. *Mineralogical Magazine*, 68(3): 467~487.
- Portela B, Sepp M D, van F J A, et al. 2021. Using hyperspectral imagery for identification of pyrophyllite muscovite intergrowths and aluminite in the shallow epithermal environment of the Yerington porphyry copper district[J]. *Ore Geology Reviews*, 131(1): 104012.
- Quan Rui, Dong Guochen, Miu Guang, et al. 2016. Zircon U-Pb ages, Hf isotopic compositions and geochemistry characteristics of the Hongshan ore-bearing syenites and their morphologies from Southern Taihang Mountains[J]. *Geological Review*, 62(4): 1 064~1 080 (in Chinese with English abstract).
- Richards J P. 2015. The oxidation state, and sulfur and Cu contents of arc magmas: Implications for metallogeny[J]. *Lithos*, 23(3): 27~45.
- Richards J P, Spell T, Rameh E, et al. 2012. High Sr/Y magmas reflect arc maturity, high magmatic water content, and porphyry Cu±Mo±Au potential: Examples from the Tethyan arcs of central and eastern Iran and western Pakistan[J]. *Economic Geology*, 107(2): 295~332.
- Schirra M, Laurent O, Zwyer T, et al. 2022. Fluid evolution at the Batu Hijau porphyry Cu-Au deposit, Indonesia: Hypogene sulfide precipitation from a single phase aqueous magmatic fluid during chlorite white-mica alteration[J]. *Economic Geology*, 117(5): 979~1 012.
- Shi Zhiwei, Dong Guochen, Gao Ting, et al. 2020. Mineralogical characteristics of Jiaochang diorite in Southern Taihang Mountains and geological significance[J]. *Earth Science*, 45(6): 2 103~2 116 (in Chinese with English abstract).
- Sillitoe R H. 1972. A plate tectonic model for the origin of porphyry copper deposits[J]. *Economic Geology*, 67(2): 184~197.
- Sillitoe R H. 2010. Porphyry copper systems[J]. *Economic Geology*, 105(1): 3~41.
- Sun W D, Huang R, Li H, et al. 2015. Porphyry deposits and oxidized magmas[J]. *Ore Geology Reviews*, 65(1): 97~131.
- Sun W D, Liang H, Ling M, et al. 2013. The link between reduced porphyry copper deposits and oxidized magmas[J]. *Geochimica et Cosmochimica Acta*, 103: 263~275.
- Tang Nan, Lin Bin, Li Yubin, et al. 2021. Application of short-wave-length infrared spectroscopy in porphyry-epithermal system: A case study of Tiegelongnan super-large copper (gold) deposit, Tibet[J]. *Acta Geologica Sinica*, 95(8): 2 613~2 627 (in Chinese with English abstract).
- Thompson A J, Hauff P L and Robitaille A J. 2009. Alteration mapping in exploration: Application of short-wave infrared (SWIR) spectroscopy[J]. *Remote Sensing and Spectral Geology*, 16: 25~40.
- Tian Chenghua, Yang Liqiang, He Wenlan, et al. 2021. Characteristics of short wave infrared spectroscopy of sericitic group minerals and their implications for exploration in the Yulong porphyry copper deposit, Tibet[J]. *Sedimentary Geology and Tethyan Geology*, 42(1): 40~49 (in Chinese with English abstract).
- Tischendorf G, Förster H J and Gottesmann B. 1999. The correlation between lithium and magnesium in trioctahedral micas: Improved equations for Li₂O estimation from MgO data[J]. *Mineralogical Magazine*, 63(1): 57~74.
- Tischendorf G, Gottesmann B, Förster H J, et al. 1997. On Li bearing micas: Estimating Li from electron microprobe analyses and an improved diagram for graphical representation[J]. *Mineralogical Magazine*, 61(409): 809~834.
- Uribe-Mogollon C and Maher K. 2018. White mica geochemistry of the copper cliff porphyry Cu deposit: Insights from a vectoring tool applied to exploration[J]. *Economic Geology*, 113(6): 1 269~1 295.
- Uribe-Mogollon C and Maher K. 2020. White mica geochemistry: Discriminating between barren and mineralized porphyry systems[J]. *Economic Geology*, 115(2): 325~354.
- Wang Baohua, Hu Rongguo, Si Jiantao, et al. 2021. Chemical variation and significance of white mica in granite porphyry from Gaofeng tin-polymetallic deposit in Dachang ore field, Guangxi[J]. *Journal of Guilin University of Technology*, 41(3): 471~483 (in Chinese with English abstract).
- Wang Chunguang, Xu Wenliang, Wang Feng, et al. 2011. Petrogenesis of the Early Cretaceous Xi'anli hornblende-gabbros from the Southern Taihang Mountains: Evidence from zircon U-Pb geochronology, Hf isotope and whole-rock geochemistry[J]. *Earth Science*, 36(3): 471~482 (in Chinese with English abstract).
- Wang Wei, Leng Chengbiao, Zhang Xingchun, et al. 2021. Mineral

- chemistry of chlorite and epidote in Diyanqinamu porphyry Mo deposit of Inner Mongolia and its implication for exploration [J]. *Mineral Deposits*, 40 (2): 241~261 (in Chinese with English abstract).
- Wang Xiaoyu, Mao Jingwen, Cheng Yanbo, et al. 2014. Characteristics of chlorite from the Xinliaodong Cu polymetallic deposit in eastern Guangdong Province and their geological significance [J]. *Acta Petrologica et Mineralogica*, 33 (5): 885~905 (in Chinese with English abstract).
- Wang Y H, Zhang F F, Liu J J, et al. 2018. Ore genesis and hydrothermal evolution of the Donggebi porphyry Mo deposit, Xinjiang, Northwest China: Evidence from isotopes (C, H, O, S, Pb), fluid inclusions, and molybdenite Re-Os dating [J]. *Economic Geology*, 113 (2): 463~488.
- Wiewióra A and Weiss Z. 1990. Crystalline chemical classifications of phyllosilicates based on the unified system of projection of chemical composition: II. The chlorite group [J]. *Clay minerals*, 25(1): 83~92.
- Wilkinson J J, Chang Z, Cooke D R, et al. 2015. The chlorite proximitator: A new tool for detecting porphyry ore deposits [J]. *Journal of Geochemical Exploration*, 152: 10~26.
- Wu D, Pan J, Xia F, et al. 2019. The mineral chemistry of chlorite and its relationship with uranium mineralization from Huangsha uranium mining area in the Middle Kunlun Range, SE China [J]. *Minerals*, 9(3): 199~227.
- Wu Fuyuan, Xu Yigang, Cao Shan, et al. 2008. Lithospheric thinning and major destruction of the North China Craton [J]. *Acta Petrologica Sinica*, 24(6): 1145~1174 (in Chinese with English abstract).
- Xi Chaozhuang, Du Gaofeng, Dai Xueling, et al. 2021. Geochemistry and chronology characteristics of Kuangshan complex in the southern Taihang Mountain and the geological significance [J]. *Contributions to Geology and Mineral Resources Research*, 36(3): 308~317 (in Chinese with English abstract).
- Xiao B and Chen H. 2020. Elemental behavior during chlorite alteration: New insights from a combined EMPA and LA-ICP-Ms study in porphyry Cu systems [J]. *Chemical Geology*, 543(2): 119~604.
- Xiao B, Chen H, Hollings P, et al. 2018. Element transport and enrichment during propylitic alteration in Paleozoic porphyry Cu mineralization systems: Insights from chlorite chemistry [J]. *Ore Geology Reviews*, 102(1): 437~448.
- Xie X, Byerly G R and Ferrell Jr R E. 1997. Ilb trioctahedral chlorite from the Barberton greenstone belt: Crystal structure and rock composition constraints with implications to geothermometry [J]. *Contributions to Mineralogy and Petrology*, 126(1): 275~291.
- Xu Wenliang and Gao Yan. 1990a. Rare earth element geochemistry of intrusive rock series of Yanshan stage from Han-Xing district, Hebei Province, China [J]. *Acta Petrologica Sinica*, 6 (2): 43~50 (in Chinese with English abstract).
- Xu Wenliang and Lin Jingqian. 1990b. The magmatic evolution of Hb-diopside series of Yanshan stage in Han-Xing district, China—The amphibole-dominated fractional crystallization [J]. *Journal of Jilin University (Earth Science Edition)*, 20(3): 259~264 (in Chinese with English abstract).
- Xu Y G. 2001. Thermo tectonic destruction of the Archaean lithospheric keel beneath the Sino-Korean Craton in China: Evidence, timing and mechanism [J]. *Physics and Chemistry of the Earth, Part A: Solid Earth and Geodesy*, 26(9~10): 747~757.
- Xue Q, Wang R, Liu S, et al. 2021. Significance of chlorite hyperspectral and geochemical characteristics in exploration. A case study of the giant Qulong porphyry Cu-Mo deposit in collisional orogen, Southern Tibet [J]. *Ore Geology Reviews*, 134: 104~156.
- Yang C, Beaudoin C, Tang J Y, et al. 2022. Cu-sulfide mineralogy, texture, and geochemistry in the Tiegelongan porphyry-epithermal copper system, Tibet, China [J]. *Mineralium Deposita*, 57: 1~21.
- Yang Changqing, Ba Yan, Wang Yanhui, et al. 2023. Ordovician magmatism in the North China Craton—Evidence from U-Pb age of the inherited zircon from Cretaceous diorite in Lingtou area, Anyang, Henan [J]. *Geological Review*, 69(3): 1150~1160 (in Chinese with English abstract).
- Yang Hang, Qin Kezhang, Wu Peng, et al. 2023. Tectonic setting, mineralization and ore-controlling factors of porphyry Cu-Mo-Au deposits [J]. *Mineral Deposits*, 42(1): 128~156 (in Chinese with English abstract).
- Yao Shixin, Wu Liangshi and Pei Rongfu. 1993. Geological, geochemical and mineralization characteristics of Hongshan intrusive complex in Handan-Xingtai Area, Hebei Province [J]. *Geology and Exploration*, 5(1): 11~16 (in Chinese with English abstract).
- Ye Meifang, Liu San, Xie Guwei, et al. 2016. Characteristics of micas from sericitolite of the Gongpoquan and Baishantang deposits, Beishan area by scanning electron microscope, X-ray diffraction and electron microprobe analyses [J]. *Rock and Mineral Analysis*, 35 (2): 166~177 (in Chinese with English abstract).
- Yin Ming, Guo Min and Zhang Haidong. 2014. Petrogenesis and evolution of Mesozoic complexes from Southern Taihang Orogen [J]. *Northwestern Geology*, 47(3): 43~53 (in Chinese with English abstract).
- Yin R, Han L, Huang X L, et al. 2019. Textural and chemical variations of micas as indicators for tungsten mineralization: Evidence from highly evolved granites in the Dahutang tungsten deposit, South Chi-

- na[J]. American Mineralogist, 104(7): 949~965.
- Zane A and Weiss Z. 1998. A procedure for classifying rock-forming chlorites based on microprobe data; Una procedura per la classificazione delle cloriti sulla base di dati microchimici[J]. Atti della Accademia Nazionale dei Lincei. Rendiconti. Scienze Fisiche e Naturali, 9.
- Zang W and Fyfe W S. 1995. Chloritization of the hydrothermally altered bedrock at the Igarapé Bahia gold deposit, Carajás, Brazil[J]. Mineralium Deposita, 30(1): 30~38.
- Zeng Shuming, Zhang Yan, Han Runsheng, et al. 2023. Characteristics and geological significance of chlorite in Wengkongba copper polymetallic deposit, southwestern Yunnan[J]. Mineral Deposits, 42(4): 828~844 (in Chinese with English abstract).
- Zhai Mingguo, Fan Qicheng, Zhang Hongfu, et al. 2005. Lower crust processes during the lithosphere thinning in eastern China: Magma underplating, replacement and delamination[J]. Acta Petrologica Sinica, 21(6): 1 509~1 526 (in Chinese with English abstract).
- Zhang Bo, Su Shangguo, Wang Guodong, et al. 2020. Mineral chemistry of clinopyroxene from the Hongshan syenite complex in Wu'an, Hebei Province: Implications for magma evolution[J]. Geology in China, 47(3): 782~797 (in Chinese with English abstract).
- Zhang Haidong, Liu Jianchao, Chen Zhengle, et al. 2014. Petrogenesis of the Pingshun complexes in the Southern Taihang Mountains: Petrology, geochronology and geochemistry[J]. Geotectonica et Metallogenia, 36(2): 454~471 (in Chinese with English abstract).
- Zhang Juan, Liu Xinxing, Wang Yitian, et al. 2021. Characteristics of chlorite from the Baguamiao gold deposit in Shaanxi Province and its geological implication[J]. Geological Bulletin of China, 40(4): 586~603 (in Chinese with English abstract).
- Zhang S, Xiao B, Long X, et al. 2020. Chlorite as an exploration indicator for concealed skarn mineralization: Perspective from the Tonglushan Cu-Au-Fe skarn deposit, Eastern China[J]. Ore Geology Reviews, 126: 103~778.
- Zhang W, Zhang F F, Wang Y H, et al. 2022. Chlorite chemistry, HOS-Pb isotopes and fluid characteristics of the Yuhai Cu-Mo Deposit in Eastern Tianshan: Implications for porphyry copper mineralization and exploration[J]. Journal of Geochemical Exploration, 241: 59~107.
- Zhang Zhanshi, Hua Renmin, Ji Junfeng, et al. 2007. Characteristics and formation conditions of chlorite in No. 201 and No. 361[J]. Acta Mineralogica Sinica, 27(2): 161~172 (in Chinese with English abstract).
- Zhao Youdong, Wu Junqi, Ling Hongfei, et al. 2016. Mineral chemistry of biotite and chlorite in western part of Fucheng granite, southern Jiangxi Province: Implications for uranium mineralization[J]. Mineral Deposits, 35(1): 153~168 (in Chinese with English abstract).
- Zhou Dong, Zhao Taiping, Zhao Pengbin, et al. 2018. Chlorite EPMA characteristic and its geological significance of the Kangshan Au-Ag-Pb-Zn deposit in west of Henan[J]. Mineral Exploration, 9(5): 803~824 (in Chinese with English abstract).
- Zhou Ling and Chen Bin. 2005. Petrogenesis and significance of the Hongshan syenite in the South Taihang Mountains: Zircon SHRIMP geochronology, chemical composition and Sr-Nd isotopic characteristics[J]. Progress in Natural Science, 11(1): 1 357~1 365 (in Chinese with English abstract).
- ## 附中文参考文献
- 艾永富, 刘国平. 1998. 内蒙大井矿床的绿泥石研究[J]. 北京大学学报(自然科学版), 34(1): 99~107.
- 白富生. 2022. 冀南邯郸地区洪山杂岩体成因及其成矿作用的研究[D]. 石家庄: 河北地质大学.
- 常浩, 张良良, 岳鹏. 2020. 邯郸市洪山沟铜矿地质特征及成因初探[J]. 中国金属通报, (1): 37, 39.
- 常浩, 张良良, 岳鹏, 等. 2017. 河北省武安市洪山沟铜及多金属矿普查报告[R]. 河北省第九地质大队.
- 陈衍景, 倪培, 范宏瑞, 等. 2007. 不同类型热液金矿系统的流体包裹体特征[J]. 岩石学报, 23(9): 2 085~2 108.
- 楚翔凯, 申萍, 李昌昊, 等. 2023. 内蒙古乌努格吐山斑岩铜钼矿床成矿流体演化——基于短波红外光谱、云母成分和石英流体包裹体研究[J]. 岩石学报, 39(11): 3 461~3 478.
- 崔晓亮, 苏尚国, 张雅南, 等. 2022. 河北太行山南段符山杂岩体岩浆作用深部过程及其大地构造意义[J]. 地学前缘, 29(1): 342~363.
- 付建刚, 李光明, 郭伟康, 等. 2023. 西藏拉隆穹窿淡色花岗岩中白云母矿物地球化学特征及对稀有金属成矿的指示[J]. 东华理工大学学报(自然科学版), 46(6): 555~575.
- 葛祥坤, 句海玉, 赵峰华, 等. 2020. 内蒙古上打井斑岩型钼矿床绿泥石特征及成矿意义[J]. 地质与勘探, 56(4): 704~713.
- 耿国建, 马宝军, 申方乐. 2023. 太行山南段桃园铜矿地质特征及成矿作用[J]. 河北地质大学学报, 46(4): 90~100.
- 郭娜, 黄一入, 郑龙, 等. 2017. 高硫-低硫化浅成低温热液矿床的短波红外矿物分布特征及找矿模型——以西藏铁格隆南(荣那矿段)、斯弄多矿床为例[J]. 地球学报, 38(5): 767~778.
- 郭国林, 刘晓东, 潘家永, 等. 2012. 302 铀矿床绿泥石特征及其与铀成矿的关系[J]. 铀矿地质, 28(1): 35~41.
- 贺文, 林彬, 宋英昕, 等. 2023. 西藏铁格隆南超大型铜(金)矿床白云母矿物学特征及地质意义[J]. 地质学报, 97(6): 1 938~1 955.
- 侯增谦, 潘小菲, 杨志明, 等. 2007. 初论大陆环境斑岩铜矿[J]. 现代地质, 21(2): 332~351.

- 李发桥, 唐菊兴, 宋扬, 等. 2024. 藏西北多龙矿集区拿若斑岩铜(金)矿床磷灰石矿物学特征及地质意义[J]. 地质论评, 70(3): 885~906.
- 李进文, 张德全, 赵士宝, 等. 2006. 得尔布干成矿带西南段金属成矿规律及找矿方向[J]. 矿床地质, 25(S1): 19~22.
- 李随民, 李玉成, 赵淑梅, 等. 2022. 河北邯郸洪山铜矿 Ar-Ar 和 U-Pb 年龄及其对成矿时代的限定[J]. 中国地质, 49(2): 575~585.
- 李玉成, 贾立芹, 赵书梅, 等. 2016. 太行山南段洪山火山机构岩相特征[J]. 现代矿业, 32(5): 142~145.
- 李紫烨, 邢欢, 李随民, 等. 2017. 娄里金矿床包裹体测试及地质意义[J]. 地质找矿论丛, 32(2): 205~213.
- 刘松岩, 张达, 杨明建, 等. 2024. 熊耳山矿集区蒿坪 Ag-Au 多金属矿床绿泥石特征及其找矿意义[J]. 地质力学学报, 30(1): 129~146.
- 刘昕曜. 2016. 太行山南段洪山正长斑岩成岩成矿作用[D]. 北京: 中国地质大学(北京).
- 马万伟, 黄小龙, 于洋, 等. 2020. 栗木花岗岩中云母的特征: 对锡成矿热液作用过程的指示[J]. 大地构造与成矿学, 44(6): 1143~1159.
- 权瑞, 董国臣, 缪广, 等. 2016. 太行山南段洪山矿化正长斑岩 LA-ICP-MS 锆石 U-Pb 年龄、Hf 同位素组成及地球化学特征[J]. 地质论评, 62(4): 1064~1180.
- 史志伟, 董国臣, 高庭, 等. 2020. 太行山南段教场闪长岩矿物学特征及其成矿意义[J]. 地球科学, 45(6): 2103~2116.
- 唐楠, 林彬, 陈玉林, 等. 2021. 短波红外光谱技术在斑岩-高硫化型浅成低温热液矿床中的应用——以西藏铁格隆南超大型铜(金)矿床为例[J]. 地质学报, 95(8): 2613~2627.
- 田成华, 杨立强, 和文言, 等. 2022. 西藏玉龙斑岩铜矿床绢云母族蚀变矿物短波红外光谱特征及对勘查的指示意义[J]. 沉积与特提斯地质, 42(1): 40~49.
- 王葆华, 胡荣国, 司建涛, 等. 2021. 广西大厂矿田高峰锡多金属矿床花岗斑岩白云母化学特征及其地质意义[J]. 桂林理工大学学报, 41(3): 471~483.
- 王春光, 许文良, 王枫, 等. 2011. 太行山南段西安里早白垩世角闪辉长岩的成因: 锆石 U-Pb 年龄、Hf 同位素和岩石地球化学证据[J]. 地球科学, 36(3): 471~482.
- 王伟, 冷成彪, 张兴春, 等. 2021. 内蒙古迪彦钦阿木斑岩铜矿床绿泥石和绿帘石矿物化学特征及其成矿指示意义[J]. 矿床地质, 40(2): 241~261.
- 王小雨, 毛景文, 程彦博, 等. 2014. 广东新寮崇铜多金属矿床绿泥石特征及其地质意义[J]. 岩石矿物学杂志, 33(5): 885~905.
- 吴福元, 徐义刚, 高山, 等. 2008. 华北岩石圈减薄与克拉通破坏研究的主要学术争论[J]. 岩石学报, 24(6): 1145~1174.
- 息朝庄, 杜高峰, 戴雪灵, 等. 2021. 太行山南段矿山杂岩体 LA-ICP-MS 锆石 U-Pb 年代学、地球化学及其地质意义[J]. 地质找矿论丛, 36(3): 308~317.
- 许文良, 高燕. 1990a. 邯郸地区燕山期侵入岩系的稀土元素特征[J]. 岩石学报, 6(2): 43~50.
- 许文良, 林景仟. 1990b. 邯郸地区燕山期角闪长岩系的岩浆演化——角闪石占主导的矿物分离结晶作用[J]. 长春地质学院学报, 20(3): 259~264.
- 杨长青, 巴燕, 王艳慧, 等. 2023. 华北克拉通奥陶纪岩浆活动——来自河南安阳岭头地区白垩纪闪长岩中继承锆石 U-Pb 年龄的证据[J]. 地质论评, 69(3): 1150~1160.
- 杨航, 秦克章, 吴鹏, 等. 2023. 斑岩铜-钼-金矿床: 构造环境、成矿作用与控制因素[J]. 矿床地质, 42(1): 128~156.
- 姚士新, 吴良士, 裴荣富. 1993. 河北邯山区洪山岩体地质地球化学及铜(金)矿化特征[J]. 地质勘探, 5(1): 11~16.
- 叶美芳, 刘三, 解巍, 等. 2016. 应用扫描电镜-X射线衍射-电子探针研究大山斑岩铜矿带角英岩中白色云母的特征[J]. 岩矿测试, 35(2): 166~177.
- 明郭敏, 张海东. 2014. 太行山南段中生代杂岩体成因及其演化分析[J]. 西北地质, 47(3): 43~53.
- 曾淑明, 张艳, 韩润生, 等. 2023. 滇西南翁孔坝铜多金属矿床绿泥石特征及其地质意义[J]. 矿床地质, 42(4): 828~844.
- 翟明国, 樊祺诚, 张宏福, 等. 2005. 华北东部岩石圈减薄中的下地壳过程: 岩浆底侵、置换与拆沉作用[J]. 岩石学报, 21(6): 1509~1526.
- 张波, 苏尚国, 王国栋, 等. 2020. 河北武安洪山正长岩杂岩体中单斜辉石矿物成分特征与岩浆演化过程[J]. 中国地质, 47(3): 782~797.
- 张海东, 刘建朝, 陈正乐, 等. 2014. 太行山南段平顺杂岩体成因: 岩石学、年代学和地球化学证据[J]. 大地构造与成矿学, 38(2): 454~471.
- 张娟, 刘新星, 王义天, 等. 2021. 陕西凤太矿集区八卦庙金矿床绿泥石特征及其找矿意义[J]. 地质通报, 40(4): 586~603.
- 张展适, 华仁民, 季峻峰, 等. 2007. 20 和 361 铀矿床中绿泥石的特征及其形成环境研究[J]. 矿物学报, 27(2): 161~172.
- 赵友东, 吴俊奇, 凌洪飞, 等. 2016. 赣南富城岩体黑云母及其蚀变产物绿泥石的矿物化学研究——对铀成矿的指示意义[J]. 矿床地质, 35(1): 153~168.
- 周栋, 赵太平, 赵鹏彬, 等. 2018. 豫西康山金银铅锌矿床绿泥石电子探针成分特征及其地质意义[J]. 矿产勘查, 9(5): 803~824.
- 周凌, 陈斌. 2005. 南太行洪山正长岩体的成因和意义: 锆石 SHRIMP 年代学、化学成分和 Sr-Nd 同位素特征[J]. 自然科学进展, 11(1): 1357~1365.